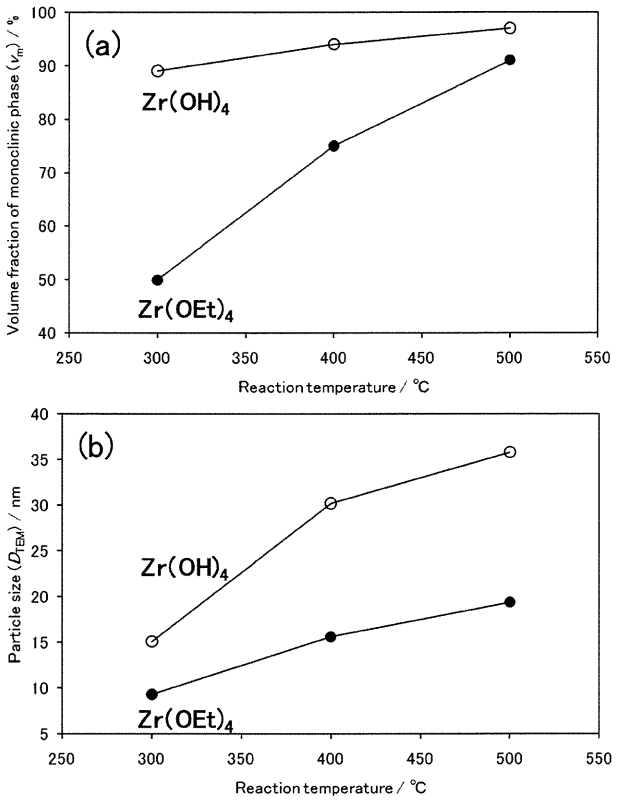

Fig. 3 (a) Plot of the volume fraction of the monoclinic phase (v_m) and (b) particle size (D_{TEM}) of ZrO_2 nanoparticles *vs.* reaction temperature synthesized from (●) $Zr(OEt)_4$ and (○) $Zr(OH)_4$.

between 800 and 400 cm^{-1}.[39,40] In **OEt-200** and **OH-200**, distinctive absorption bands of ZrO_2 are not shown in this region. In **OEt-** and **OH-300–500**, two distinctive bands with two peaks around 750 and 500 cm^{-1} were observed, which are assigned to the Zr–O modes in monoclinic ZrO_2.[39,40] Notably, these peaks of **OEt**-series were pronounced with higher reaction temperatures, which is consistent with the XRD results.

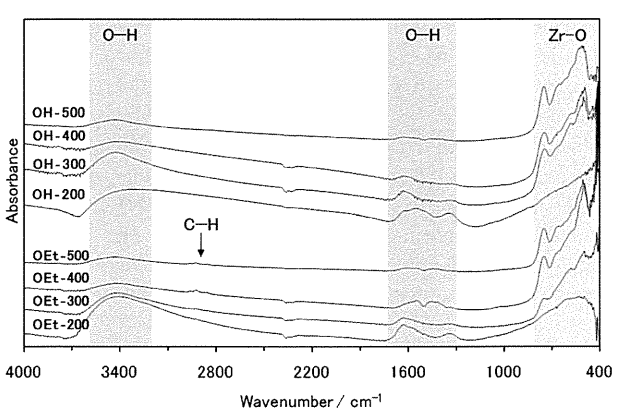

Fig. 4 FT-IR spectra of the products synthesized from $Zr(OEt)_4$ at 200 °C (**OEt-200**); 300 °C (**OEt-300**); 400 °C (**OEt-400**) and 500 °C (**OEt-500**), synthesized from $Zr(OH)_4$ at 200 °C (**OH-200**); 300 °C (**OH-300**); 400 °C (**OH-400**) and 500 °C (**OH-500**).

Some distinctive bands were observed in the spectra of the products besides the Zr–O bands. A broad band between 3600 and 3200 cm^{-1} and some distinctive bands between 1700 and 1250 cm^{-1} were shown in all the spectra. They are assigned to the O–H modes of chemisorbed water and terminated hydroxides.[41,42] These results are reasonable to suggest that the water and/or hydroxide group are chemisorbed at the surface of the products. The chemisorbed water and the hydroxide group possibly existed in the products because of the hydrothermal method. The chemisorbed water and terminated hydroxides are considered to coordinate to the Zr ions, and it seems to cause the lattice defects at the surface of the products. The intensity of the O–H bands is weakened for the products synthesized at higher temperature; it is prominent especially for the band between 3600 and 3200 cm^{-1}. The weakened intensity of the bands indicates a decrease in the amount of the chemisorbed water and the terminated hydroxides. The decrease is due to the decrease in the surface-to-volume ratio of the grown products (nanoparticles). These results also suggest that the amount of the chemisorbed water and/or the terminated hydroxides depends on the reaction temperature and the particle size rather than the difference in the precursor. The bands between 1700 and 1250 cm^{-1} depended on the products; the bands shifted between **OEt-300** and **-400** and **OH-200** and **-300**. From the XRD data, it is clear that the surface condition seems to be different among the amorphous, the tetragonal, and the monoclinic phases of ZrO_2. However, a clear explanation was difficult to give from this result only. The difference in the precursor that affects the phase contents in the products is thought to influence the FT-IR spectra of the products. On the other hand, **OEt-500** and **OH-500** with close volume fractions and different particle size show similar spectra. Therefore, the quality like the crystallinity of the monoclinic ZrO_2 did not depend on the precursor. This is consistent with the trend shown in the data of the lattice parameters.

Incidentally, weak bands around 3000 and 2800 cm^{-1} were shown in **OEt-200–500**, which are assigned to the C–H modes of the ethoxy group in $Zr(OEt)_4$ as the impurity bands for the products.[41] As mentioned previously, the precursor-dependent phenomena were contributed by the difference in the influence of the counter anions of the precursors. The phase transition rate of **OEt**-series was slower than that of **OH**-ones. The slow rate of **OEt**-series might be due to the presence of the ethoxy group.

The UV-Vis powder diffuse reflectance spectra of all the products are shown in Fig. 5. All the spectra showed an absorption edge around 5.0 eV and a broad absorption in the region between 3.0 and 5.0 eV. The absorption edge around 5.0 eV corresponds to the optical band gap for ZrO_2.[13,16,43] The band gaps of all the products were roughly estimated from the absorption edge. The band gaps of **OEt-200** and **OH-200** were 4.9 and 4.7 eV, respectively. They are probably affected by the edge broadening that originated in the amorphous phase.[44,45] The band gaps of the other products (**OEt-** and **OH-300–500**) were about 5.1 eV. According to Fig. 1, **OH-500** is a single phase of the monoclinic ZrO_2, so that the band gap of it is assigned to the monoclinic one. Based on this concept, the estimated band gaps of **OEt-300–500** and **OH-300–400** are also probably originated in the monoclinic ZrO_2. The broad absorption tail below 5.0 eV in all the spectra is thought to be due to the influence of the lattice defects like interstitial defects, oxygen vacancies, and/or valence

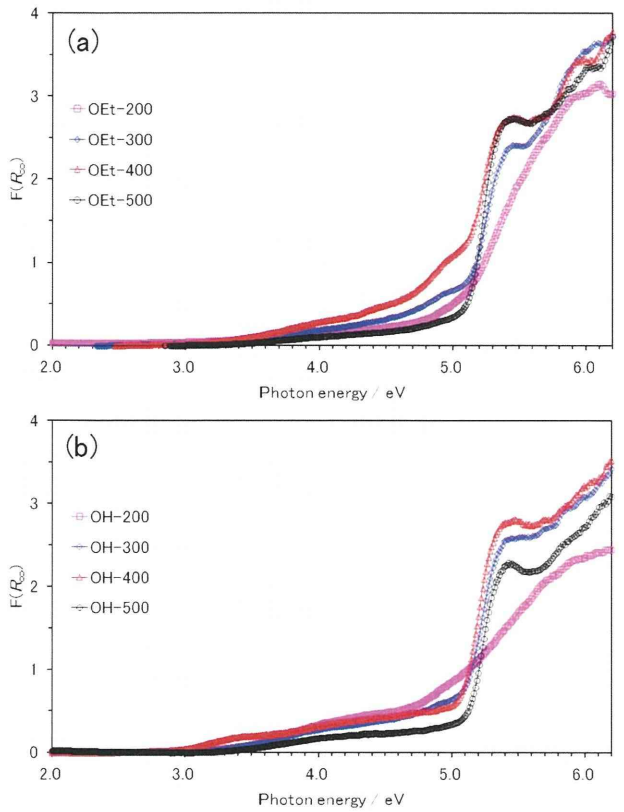

Fig. 5 UV-Vis powder diffuse reflectance spectra of the products synthesized from (a) $Zr(OEt)_4$ at 200 °C (pink, □: **OEt-200**); 300 °C (blue, ◇: **OEt-300**); 400 °C (red, △: **OEt-400**) and 500 °C (black, ○: **OEt-500**); (b) $Zr(OH)_4$ at 200 °C (pink, □: **OH-200**); 300 °C (blue, ◇: **OH-300**); 400 °C (red, △: **OH-400**) and 500 °C (black, ○: **OH-500**).

change of Zr ions, because these lattice defect levels are formed in the band gap region.[46–48] The conditions of the chemisorbed water and the terminated hydroxides were dependent on the products and they have the possibility to degrade the crystallinity at the surface of the products. However, the change in the intensity of this tail area was not consistent with the trend shown in Fig. 4. It seems to depend on the phase content and/or the particle size of the products rather than the amount of the chemisorbed water and the terminated hydroxides. Thus, the reason for the tail area of the UV-Vis spectra is thought to be due to the low crystallinity of the nanoparticles with high surface area. Note that the estimated band gaps of **OEt-** and **OH-300–500** are lower than those of bulk ZrO_2 samples.[43,49,50] This trend in our products is similar to that of other nanoparticles.[13,16] The existence of the tail area is considered to influence the accuracy of the estimation. Considering the data accuracy, it is believed that no remarkable difference in the estimated band gaps of **OEt-** and **OH-300–500** was found. The optical property of the products is less influenced by the precursor, which is consistent with the trend shown in the data of the lattice parameters and the FT-IR spectra.

Summary

In this study we synthesized ZrO_2 nanoparticles from $Zr(OEt)_4$ and $Zr(OH)_4$ as the precursors by the hydrothermal method using sub- or supercritical water at temperatures between 200 and 500 °C for 10 min. The products synthesized at higher temperatures over 300 °C showed mixtures of tetragonal and monoclinic phases, while the product synthesized at 200 °C showed the amorphous phase. The volume fraction of the monoclinic phase increased for the products synthesized at higher temperature. This trend was the same for both **OEt-** and **OH-**series; however, $Zr(OH)_4$ was found to be better than $Zr(OEt)_4$ for obtaining products with high volume fraction of the monoclinic phase. ZrO_2 nanoparticles obtained from $Zr(OH)_4$ and heat treated at 500 °C showed a single phase of monoclinic crystal structure. The particle size of the products was found to depend on the type of precursors. The particle size of the monoclinic phase increased for the product synthesized at higher temperatures, although the particle size of the **OEt-**series was smaller than that of the **OH-**ones under the same conditions. The reaction temperature and the precursor are important for controlling the crystalline phase and the particle size of the products.

Both the products synthesized from different precursors had chemisorbed water and a hydroxide group, which are thought to exist at the surface of the products. The chemisorbed water and the hydroxide group in the products were formed during the hydrothermal synthesis. Their amount depends on the reaction temperature rather than the precursor of the hydrothermal method. The optical band gaps of the products were also roughly estimated, but significant differences were not seen among the products synthesized from different precursors. Therefore, we concluded that the difference in the precursor does not affect the quality in terms of the crystallinity of the products. Experimental results in the present work reveal that the selection of the precursor and tuning of the reaction temperature enable us to control the crystalline phase and the particle size of the ZrO_2 nanoparticles prepared by the simple and rapid hydrothermal method presented here. We believe that the results of this study will contribute to mass production of ZrO_2 nanoparticles.

Acknowledgements

This work was supported by a Grant-in-Aid for Scientific Research (S) (KAKENHI) no. 20226015.

References

1 E. C. Subbarao, H. S. Maiti and K. K. Srivastava, *Phys. Status Solidi A*, 1974, **21**, 9–40.
2 M. Yashima, T. Kato, M. Kakihana, M. A. Gulgun, Y. Matsuo and M. Yoshimura, *J. Mater. Res.*, 1997, **12**, 2575–2583.
3 J. Schefold, A. Brisse and M. J. Zahid, *J. Electrochem. Soc.*, 2009, **156**, B897–B904.
4 J. H. Shin, C.-C. Chao, H. Huang and F. B. Prinz, *Chem. Mater.*, 2007, **19**, 3850–3854.
5 R. C. Garvie, R. H. J. Hannink and R. T. Pascoe, *Nature*, 1975, **258**, 703–704.
6 R. H. J. Hannink, P. M. Kelly and B. C. J. Muddle, *J. Am. Ceram. Soc.*, 2000, **83**, 461–487.
7 D. He, Y. Ding, H. Luo and C. Li, *J. Mol. Catal. A: Chem.*, 2004, **208**, 267–271.
8 C.-M. Wang, K.-N. Fan and Z.-P. Liu, *J. Am. Chem. Soc.*, 2007, **129**, 2642–2647.
9 J. W. Bae, J. Y. Park, S. W. Hwang, G. Y. Yeom, K. D. Kim, Y. A. Cho, J. S. Jeon and D. Choi, *J. Electrochem. Soc.*, 2000, **147**, 2380–2384.

10 C. León, M. L. Lucia and J. Santamaría, *Phys. Rev. B: Condens. Matter Mater. Phys.*, 1997, **55**, 882–887.
11 L. Ouyang and W. Y. Ching, *J. Appl. Phys.*, 2004, **95**, 7918–7924.
12 G. D. Wilk, R. M. Wallace and J. M. Anthony, *J. Appl. Phys.*, 2001, **89**, 5243–5275.
13 K. Sato, H. Abe and S. Ohara, *J. Am. Chem. Soc.*, 2010, **132**, 2538–2539.
14 H. Hayashi, A. Ueda, A. Suino, K. Hiro and Y. Hakuta, *J. Solid State Chem.*, 2009, **182**, 2985–2990.
15 N. Zhao, D. Pan, W. Nie and X. Ji, *J. Am. Chem. Soc.*, 2006, **128**, 10118–10124.
16 J. Joo, T. Yu, Y. W. Kim, H. M. Park, F. Wu, J. Z. Zhang and T. Hyeon, *J. Am. Chem. Soc.*, 2003, **125**, 6553–6557.
17 M. Taguchi, S. Takami, T. Naka and T. Adschiri, *Cryst. Growth Des.*, 2009, **9**, 5297–5303.
18 M. Taguchi, S. Takami, T. Adschiri, T. Nakane, K. Sato and T. Naka, *CrystEngComm*, 2011, **13**, 2841–2848.
19 T. Mousavand, T. Naka, K. Sato, S. Ohara, M. Umetsu, S. Takami, T. Nakane, A. Matsushita and T. Adschiri, *Phys. Rev. B: Condens. Matter Mater. Phys.*, 2009, **79**, 144411.
20 S. Takami, S. Ohara, T. Adschiri, Y. Wakayama and T. Chikyow, *Dalton Trans.*, 2008, 5442–5446.
21 T. Adschiri, K. Kanazawa and K. Arai, *J. Am. Ceram. Soc.*, 1992, **75**, 1019–1022.
22 Y. Arai, T. Sako and Y. Takebayashi, *Supercritical Fluids*, Springer, Berlin, 2001.
23 Y.-P. Sun, *Supercritical Fluid Technology in Materials Science and Engineering*, Marcel Dekker, New York, 2002.
24 H. Toraya, M. Yoshimura and S. Somiya, *J. Am. Ceram. Soc.*, 1984, **67**, c119–c121.
25 H. Miura, *J. Crystallogr. Soc. Jpn.*, 2003, **45**, 145–147.
26 A. E. Morales, E. S. Mora and U. Pal, *Rev. Mex. Fis. S*, 2007, **53**, 18–22.
27 E. Tani, M. Yoshimura and S. Somiya, *J. Am. Ceram. Soc.*, 1981, **64**, C-181.
28 E. Tani, M. Yoshimura and S. Somiya, *J. Am. Ceram. Soc.*, 1983, **66**, 11–14.
29 R. P. Denkewicz, K. S. TenHuisen and J. H. Adair, *J. Mater. Res.*, 1990, **5**, 2698–2705.
30 Y. Murase and E. Kato, *J. Am. Ceram. Soc.*, 1983, **66**, 196–353.
31 R. T. Morrison and R. N. Boyd, *Organic Chemistry*, Prentice-Hall, New York, 1992.
32 A. Clearfield, *J. Mater. Res.*, 1990, **5**, 161–162.
33 G. T. Mamott, P. Barnes, S. E. Tarling, S. L. Jones and C. J. Norman, *J. Mater. Sci.*, 1991, **26**, 4054–4061.
34 Y. Gao and K. Koumoto, *Cryst. Growth Des.*, 2005, **5**, 1983–2017.
35 Y. Gao, F. Zhao, Y. Liu and H. Luo, *CrystEngComm*, 2011, **13**, 3511–3514.
36 M. Yoshimura, T. Noma, K. Kawabata and S. Somiya, *J. Mater. Sci. Lett.*, 1987, **6**, 465–467.
37 S. Wada and K. Yokoyama, *J. Ceram. Soc. Jpn.*, 1999, **107**, 92–95.
38 R. C. Garvie, *J. Phys. Chem.*, 1978, **82**, 218–224.
39 C. M. Phillippi and K. S. Mazdiyasni, *J. Am. Ceram. Soc.*, 1971, **54**, 254–259.
40 T. Y. Steng, C. C. Lin and J. T. Liaw, *J. Mater. Sci.*, 1987, **22**, 965–972.
41 K. Nakanishi, *Infrared Absorption Spectroscopy: Practical*, Holden-Day, San Francisco, 1962.
42 K. Nakamoto, *Infrared and Raman Spectra of Inorganic and Coordination Compounds*, Wiley, New York, 1997.
43 C.-K. Kwok and C. R. Aita, *J. Appl. Phys.*, 1989, **66**, 2756–2758.
44 Y. Gao, Y. Masuda, T. Yonezawa and K. Koumoto, *J. Ceram. Soc. Jpn.*, 2002, **110**, 379–385.
45 Y. Gao, Y. Masuda, H. Ohta and K. Koumoto, *Chem. Mater.*, 2004, **16**, 2615–2622.
46 A. S. Foster, V. B. Sulimov, F. Lopez Gejo, A. L. Shluger and R. M. Nieminen, *J. Non-Cryst. Solids*, 2002, **303**, 101–107.
47 C. Morant, A. Fernández, A. R. González-Elipe, L. Soriano, A. Stampfl, A. M. Bradshaw and J. M. Sanz, *Phys. Rev. B: Condens. Matter Mater. Phys.*, 1995, **52**, 11711–11720.
48 A. Emeline, G. V. Kataeva, A. S. Litke, A. V. Rudakova, V. K. Ryabchuk and N. Serpone, *Langmuir*, 1998, **14**, 5011–5022.
49 R. H. French, S. J. Glass, F. S. Ohuchi, Y.-N. Xu and W. Y. Ching, *Phys. Rev. B: Condens. Matter Mater. Phys.*, 1994, **49**, 5133–5142.
50 B. Králik, E. K. Chang and S. G. Louie, *Phys. Rev. B: Condens. Matter Mater. Phys.*, 1998, **57**, 7027–7036.

CrystEngComm

Dynamic Article Links

Cite this: *CrystEngComm*, 2012, **14**, 2132

www.rsc.org/crystengcomm

PAPER

Synthesis of surface-modified monoclinic ZrO_2 nanoparticles using supercritical water†

Minori Taguchi,*[a] Seiichi Takami,[b] Tadafumi Adschiri,[c] Takayuki Nakane,[a] Koichi Sato[a] and Takashi Naka[a]

Received 23rd October 2011, Accepted 9th December 2011
DOI: 10.1039/c2ce06409j

We succeeded in simple and rapid synthesis of surface-modified monoclinic ZrO_2 nanoparticles using a supercritical hydrothermal method. The precursor $Zr(OH)_4$ was treated in the presence of various surface modifiers with carboxyl group (–COOH) in a batch-type reactor at 400 °C for 10 min. Oleic, sebacic, dodecanedioic, and 12-aminododecanoic acids were used as surface modifiers. Addition of surface modifiers resulted in smaller particle (crystallite) sizes than the unmodified nanoparticles, suggesting that there is an interaction between the surface modifiers and the nanoparticles. The reduced particle size in the presence of surface modifiers was attributed to the inhibition of the growth of the crystalline surface due to the surface modification. The FT-IR spectra revealed that the surface modifiers were attached to the surface of the nanoparticles through coordination bonds between the carboxylate group ($-COO^-$) and the Zr ion. The FT-IR spectra also confirmed the presence of functional groups, such as methyl ($-CH_3$), carboxyl (–COOH), and amine ($-NH_2$), at the surface. The surface modification was also verified by the thermogravimetric analysis. The number of the surface modifiers attached to the surface of the products was about 2 molecules per nm^2. The nanoparticles with carboxyl and amine surface functional groups were water dispersible; the isoelectric point shifted to low pH ranges because of the nature of the groups.

Introduction

Organic–inorganic hybrid nanoparticles have attracted great interest because they exhibit novel properties, which are combinations of the properties of organic molecules coupled with the physical properties of the inorganic nanoparticles.[1–11] In particular, the crystallite size and consequently the particle size and/or the morphology of the hybrid nanoparticles are controlled and/or tuned by the organic molecules. The physical properties of the inorganic nanoparticles are anomalous with controlling the particle size or the morphology. Further, the presence of organic molecules on the surface of the nanoparticles improves the thermal stability and the solvent dispersibility.[1–11] The presence of free functional groups, such as carboxyl and amine, at the surface of the nanoparticles allows further conjugation with various organic compounds *via* chemical bonds, which will contribute to synthesize novel functional nanomaterials.[5–11]

Zirconium oxide (ZrO_2) has several crystalline phases, *i.e.*, amorphous, metastable tetragonal, monoclinic, tetragonal, and cubic phases.[12,13] Each of the crystalline phases possesses attractive functional properties; therefore ZrO_2 has found wide application in numerous technological fields.[14–21] Among the crystalline phases, the monoclinic ZrO_2 is thermodynamically stable below 1170 °C, and has been studied extensively for its application in catalysts or catalyst supports,[18,19] gate dielectrics,[20] and bioactive coatings on bone implants.[21] For these applications, ZrO_2 is fabricated with various forms like single crystal, thin film, nanoparticle, and as polycrystalline bulk. Notably, the preparation of ZrO_2 nanoparticles is one of the important topics of research because of its applicability in high-surface area catalysts, optical and electronic nanodevices,[22–25] wherein controlling the crystalline phase and the particle size is of utmost importance. Wet processes, such as solvo- or hydrothermal methods, in the presence of organic molecules are generally utilized as the synthesis technique for preparation of ZrO_2 nanoparticles. However, most of the published literature focused only on optimizing the experimental conditions and the techniques for synthesizing nanoparticles with controlled crystalline phases and particle sizes; little has been discussed about the

[a]*National Institute for Materials Science, 1-2-1 Sengen, Tsukuba, 305-0047, Japan. E-mail: TAGUCHI.Minori@nims.go.jp*
[b]*Institute of Multidisciplinary Research for Advanced Materials, Tohoku University, 2-1-1 Katahira, Aoba-ku, Sendai, 980-8577, Japan*
[c]*WPI, Advanced Institute for Materials Research, Tohoku University, 2-1-1 Katahira, Aoba-ku, Sendai, 980-8577, Japan*

† Electronic supplementary information (ESI) available: FT-IR spectra of original organic modifiers were shown. See DOI: 10.1039/c2ce06409j

interactions between the organic molecules and the product ZrO_2.[22–25]

Utilization of supercritical water (SCW) is one of the promising approaches for establishing a simple and rapid synthesis technique in order to prepare the surface-modified metal oxide nanoparticles by the hydrothermal method.[26–30] The heating of water in a sealed vessel decreases the dielectric constant drastically near the critical point, and results in a drastic change in the solubility of inorganic substances and organic molecules.[31,32] This phenomenon is useful for faster nucleation and crystal growth of the metal oxides. Organic molecules, used to modify the surface of metal oxide nanoparticles, dissolve under these conditions. Hence, in recent years, SCW has often been employed to synthesize surface-modified metal oxide nanoparticles. Indeed, our previous works succeeded in synthesis of various surface-modified metal oxide nanoparticles.[26–30] Recently, we also succeeded in synthesizing ZrO_2 nanoparticles with controlled crystalline phase and particle sizes using the SCW method.[30] Although, $Zr(OH)_4$ is a better precursor for obtaining a monoclinic phase under the conditions, it contributes to increased crystal growth because of the high surface energy of the phase.[30,33] Therefore, it is also a challenge to inhibit crystal growth and synthesize smaller monoclinic ZrO_2 nanoparticles. There has been no report of synthesis of surface-modified monoclinic ZrO_2 nanoparticles using SCW yet.

Our previous studies indicated that the crystal growth of metal oxides was controlled by organic molecules as surface modifiers, which resulted in reducing the particle size and/or controlling the morphology.[26–29] A similar effect can also be expected for ZrO_2 synthesis. During these studies, we have utilized various organic molecules, including hydrophilic polymers, as surface modifiers for metal oxide nanoparticles.[26–29] We found that organic molecules with carboxyl group (–COOH) were generally better surface modifiers; they are attached to the surface of the nanoparticles through coordination bond between the carboxylate group ($–COO^-$) and the metal ion. In addition, organic molecules with two or more functional groups like dicarboxylic acids and hydrophilic polymers have also been utilized as surface modifiers during synthesis of nanoparticles.[26,27]

This study is the first demonstration for synthesizing surface-modified monoclinic ZrO_2 nanoparticles in a batch-type reactor using the supercritical hydrothermal method. To synthesize the nanoparticles, $Zr(OH)_4$ was used as the precursor. Various carboxylic acids, oleic, sebacic, dodecanedioic, and 12-aminododecanoic acids, were utilized as surface modifiers.

Experimental

Materials

Zirconium hydroxide ($Zr(OH)_4$) as the precursor was purchased from Aldrich. Oleic acid (OA), sebacic acid (SA), dodecanedioic acid (DA), and 12-aminododecanoic acid (12AA) as surface modifiers were purchased from Wako Chemicals. The chemical structures of the surface modifies are as shown below:

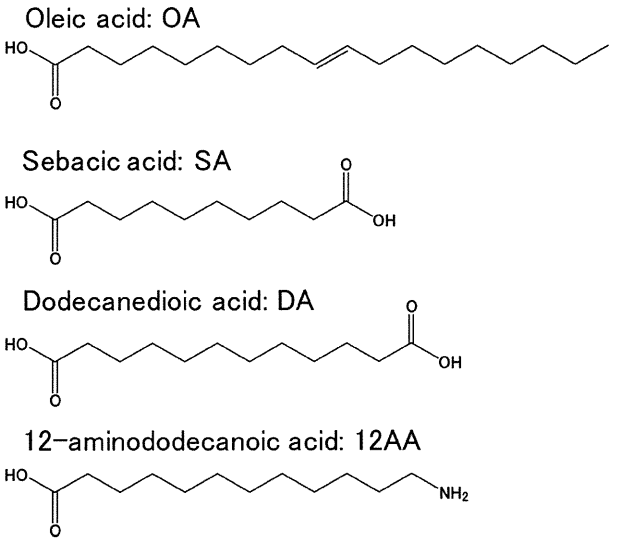

Structure of various carboxylic acids

Sample preparation

$Zr(OH)_4$ (0.25 mmol), each carboxylic acid (0.25 mmol), and distilled water (2.5 g) were transferred to a pressure-resistant Hastelloy C vessel (inner volume: 5.0 mL). The hydrothermal reactions were performed in an electric furnace at 400 °C and 38 MPa for 10 min. The reaction vessel was then quenched by submerging it into a water bath at room temperature. The solid products were then washed by a combination of repeated centrifugation and decantation, alternately with water and methanol. Finally, the products were dried in air at room temperature. Hereafter, these products were designated as (i) **OA-ZrO_2** (oleic acid (OA)-modified ZrO_2), (ii) **SA-ZrO_2** (sebacic acid (SA)-modified ZrO_2), (iii) **DA-ZrO_2** (dodecanedioic acid (DA)-modified ZrO_2), and (iv) **12AA-ZrO_2** (12-aminodecanoic acid (12AA)-modified ZrO_2). Unmodified ZrO_2 (**um-ZrO_2**) were also prepared under the same conditions (at 400 °C and 38 MPa for 10 min) without adding the modifiers.

Characterizations

X-Ray diffraction (XRD) patterns were recorded using a RINT-2000 diffractometer (Rigaku) with Cu Kα (λ = 1.542 Å) radiation at a 2θ scan speed of 2° min^{-1}. To estimate the volume fractions of the monoclinic and the tetragonal phases in the products, we calculated the ratio of the intensities of the ($\bar{1}11$) and the (111) peaks for the monoclinic phase, and that of the (101) peak for the tetragonal phases using eqn (1)–(3) as follows:[34]

$$X_m = (I_m(\bar{1}11) + I_m(111))/(I_m(\bar{1}11) + I_m(111) + I_t(101)) \quad (1)$$

$$v_m = (1.311X_m)/(1 + 0.311X_m) \quad (2)$$

$$v_t = 1 - v_m \quad (3)$$

In above equations, X_m is an intensity ratio of the monoclinic and the tetragonal phases; $I_m(\bar{1}11)$ and $I_m(111)$ are the intensities

of the ($\bar{1}11$) and the (111) peaks for the monoclinic phase, respectively; $I_t(101)$ is the intensity of the (101) peak for the tetragonal phase; v_m and v_t are the volume fractions of the monoclinic and the tetragonal phases, respectively. The lattice parameters were calculated from the XRD patterns of the products using a unit cell parameter refinement program (Cell Calc).[35] The Scherrer equation was used to determine the crystallite size of the products from the full width at half maximum (FWHM) of the monoclinic ($\bar{1}11$) peak and a shape factor of 0.9. A transmission electron microscope (TEM, JEM-1200EX, JEOL) was used to obtain the magnified image of the products. The arithmetic mean particle diameter and the size distribution were estimated from the TEM images. Additionally, the volume weighted average of the particle diameter was also calculated from the arithmetic mean particle diameter of the products.[27]

Fourier transform infrared (FT-IR) spectra were recorded using a FT/IR-680 Plus (JASCO) with KBr pellets. Thermogravimetric analysis (TGA) was performed at a temperature range from room temperature to 800 °C at a ramp rate of 10 °C min^{-1} under an argon atmosphere using a DTG-60H (Rigaku). The number of surface modifiers attached to the surface of one ZrO_2 nanoparticle was estimated using the weight loss at 800 °C, the particle size estimated from TEM images, and the density of monoclinic (JCPDS Card no. 83-0944: 5.838 g cm^{-3}) and tetragonal (JCPDS Card no. 80-0965: 6.117 g cm^{-3}) ZrO_2.[26,27] Herein, the entire surface of a particle was perfectly attached with the organic modifiers, and the morphology of the particle was spherical in shape. Zeta potentials were measured in water with a Zetasizer system (MPT-2, Malvern Instruments). The pH of suspensions was adjusted to values ranging from 3 to 11 in increments of 1, and was controlled by addition of appropriate amounts of 0.1 M HCl and KOH solutions.

Results and discussion

(1) XRD patterns and TEM images

Fig. 1 shows the XRD patterns of the ZrO_2 nanoparticle produced using the supercritical hydrothermal method. All the products mainly showed monoclinic structure (JCPDS no. 83-0944), although traces of tetragonal structure were also found. The volume fraction of the crystalline phase, the lattice parameters, and the crystallite size of the products are summarized in Table 1. The volume fraction of the monoclinic phase in all the products was above 92%. The lattice parameters did not show any remarkable difference among the products. Therefore, the crystallinity of the monoclinic ZrO_2 appears to be independent of the surface modification, even though differences in the crystallite size between products prepared with and without addition of surface modifiers were apparent. The crystallite size of the products decreased with addition of the surface modifiers when compared with **um-ZrO_2** produced without adding the surface modifiers.

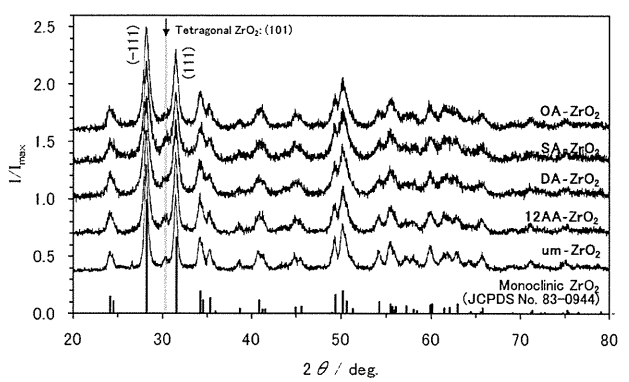

Fig. 1 XRD patterns of the products: (**OA-ZrO_2**) oleic acid-modified; (**SA-ZrO_2**) sebacic acid-modified; (**DA-ZrO_2**) dodecanedioic acid-modified; (**12AA-ZrO_2**) 12-amiododecanoic acid-modified; (**um-ZrO_2**) unmodified and JCPDS Card no. 83-0944 as monoclinic ZrO_2.

The TEM images, the arithmetic mean particle diameters, and the size distributions of the products are shown in Fig. 2. The differences in crystallite sizes were clearly apparent from the TEM observation. The volume weighted averages of the particle diameter are shown in Table 1. The morphology of all the products appeared like distorted spheres, without any remarkable difference among the products. The decrease in particle sizes of the ZrO_2 products with addition of the surface modifiers, compared with **um-ZrO_2**, was consistent with the crystallite sizes estimated from the XRD patterns. Additionally, the products obtained by addition of the surface modifiers showed narrower size distribution than that by **um-ZrO_2**. These results suggest that there is an interaction between the nanoparticles and the organic molecules as surface modifiers. The particle sizes were believed to have reduced because of growth inhibition by the surface modifiers.

(2) FT-IR spectra

The interactions between the surface modifiers and the nanoparticles were assessed by FT-IR measurements as shown in Fig. 3. The spectra of the surface modifiers alone are shown in Fig. S1†. All the ZrO_2 products showed two distinctive bands with two peaks around 750 and 500 cm^{-1}, which are assigned to the Zr–O modes in monoclinic ZrO_2.[36] **OA-ZrO_2** showed a weak band at 2962 cm^{-1}, which is assigned to the asymmetric (ν_{as}) stretching mode of $-CH_3$ in oleic acid (OA).[37] The spectrum showed some bands at 2919, 2849 and 1453 cm^{-1}, which are assigned to the asymmetric stretching (ν_{as}), symmetric stretching (ν_s), and scissoring bending (δ_{sc}) modes of $-CH_2-$ in the alkyl chain of OA, respectively. In addition, bands at 1537 and 1408 cm^{-1} in the spectrum are assigned to the ν_{as} and ν_s modes of the carboxylate group ($-COO^-$) of OA, respectively.[26,27,37,38] These bands are also observed in other products except the ν_{as} $-CH_3$ mode. In **SA-ZrO_2**, the bands appeared at 2919 (ν_{as} $-CH_2-$), 2850 (ν_s $-CH_2-$), 1535 (ν_{as} $-COO^-$), 1450 (δ_{sc} $-CH_2-$), and 1414 (ν_s $-COO^-$) cm^{-1} of sebacic acid (SA). In **DA-ZrO_2**, they appeared at 2920 (ν_{as} $-CH_2-$), 2850 (ν_s $-CH_2-$), 1537 (ν_{as} $-COO^-$), 1453 (δ_{sc} $-CH_2-$), and 1410 (ν_s $-COO^-$) cm^{-1} of dodecanedioic acid (DA). In **12AA-ZrO_2**, they appeared at 2920 (ν_{as} $-CH_2-$), 2850 (ν_s $-CH_2-$), 1543 (ν_{as} $-COO^-$), 1461 (δ_{sc} $-CH_2-$), and 1404 (ν_s $-COO^-$) cm^{-1} of 12-aminododecanoic acid (12AA). The **um-ZrO_2** showed a distinctive broad band between 3600 and 3200 cm^{-1} and a broad band around 1600 cm^{-1}, which are assigned to the O–H modes of chemisorbed water and/or terminated hydroxides at the surface.[37,38] The presence of $-COO^-$ bands indicates that the carboxyl group of

Table 1 Volume fraction of the ratio of monoclinic and tetragonal phases, lattice parameters of monoclinic phase, the particle size from the XRD (D_{XRD}) and TEM (D_{TEM}) results of the products

Products	Volume fraction v_m/v_t[a] (%)	Lattice parameters					Particle size/nm	
		a/Å	b/Å	c/Å	β/°	V/Z/Å^3	D_{XRD}	D_{TEM}
OA-ZrO_2	95/5	5.154(4)	5.218(4)	5.323(3)	99.41	35.31	23.0	16.0
SA-ZrO_2	92/8	5.160(5)	5.203(7)	5.325(6)	99.45	35.27	19.8	12.7
DA-ZrO_2	93/7	5.161(4)	5.202(6)	5.334(5)	99.40	35.33	21.9	14.1
12AA-ZrO_2	93/7	5.160(4)	5.210(4)	5.326(4)	99.38	35.33	26.4	18.8
um-ZrO_2	94/6	5.154(2)	5.210(2)	5.322(2)	99.30	35.27	37.6	30.2
JCPDS 83-0944	100/0	5.1423	5.2000	5.3110	99.205	35.05	—	—

[a] The m and the t represent monoclinic and tetragonal phases, respectively.

the surface modifiers is attached to the surface of the ZrO_2 nanoparticles through the bidentate coordination bond of the carboxylate group ($-COO^-$) on the Zr ion.[26,27,37,38] **SA-** and **DA-ZrO_2** showed a weak band at 1707 and 1708 cm^{-1}, respectively, which are assigned to the stretching mode of the free carboxyl group (–COOH), suggesting its presence at the surface.[26,27,37]

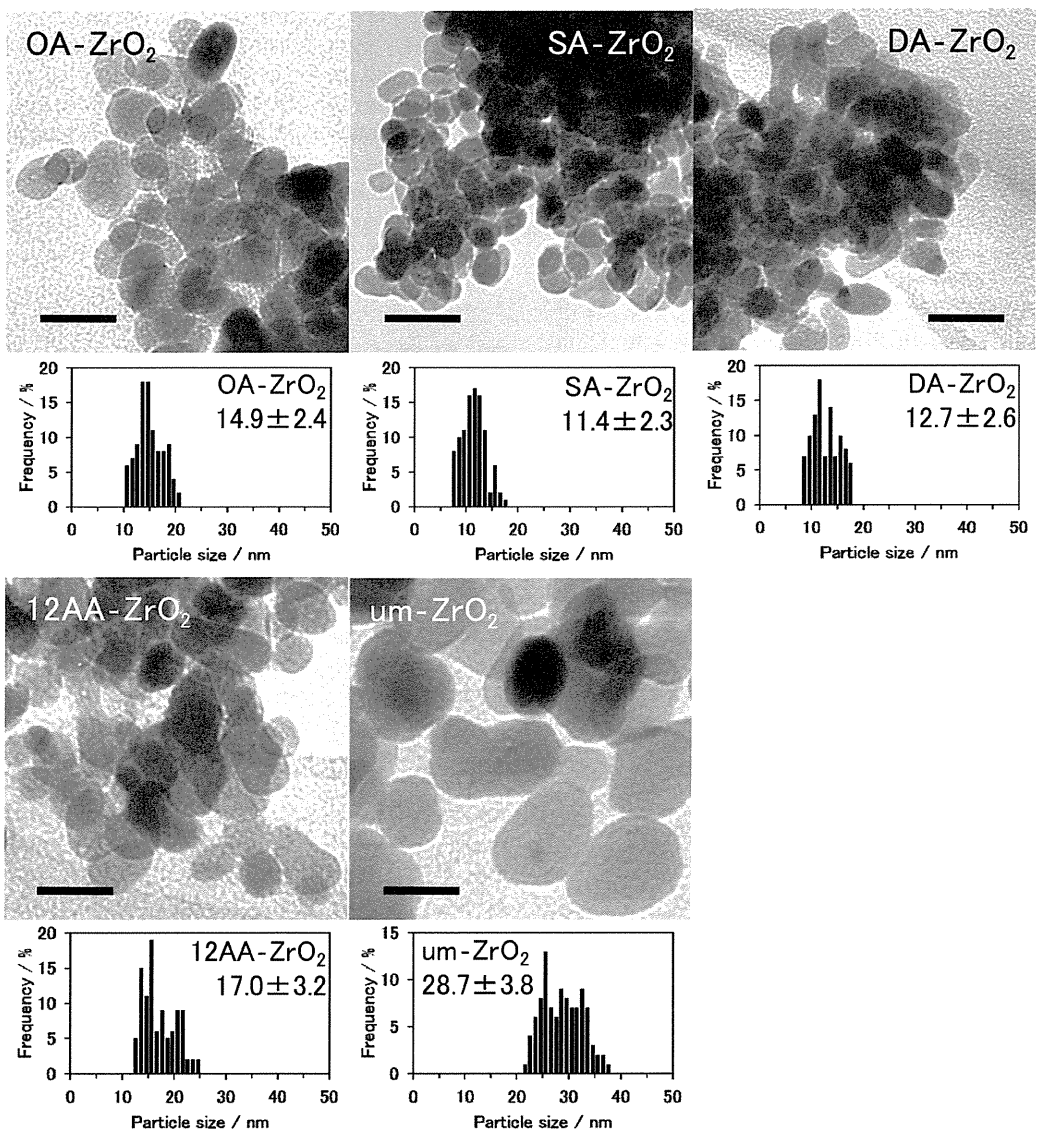

Fig. 2 TEM images, arithmetic mean particle diameters, and particle size distributions of the products: (**OA-ZrO_2**) oleic acid-modified; (**SA-ZrO_2**) sebacic acid-modified; (**DA-ZrO_2**) dodecanedioic acid-modified; (**12AA-ZrO_2**) 12-amiododecanoic acid-modified; (**um-ZrO_2**) unmodified; scale bar = 20 nm.

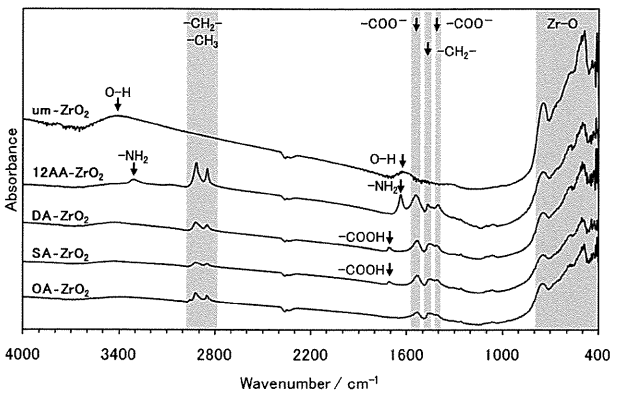

Fig. 3 FT-IR spectra of the products: (**OA-ZrO_2**) oleic acid-modified; (**SA-ZrO_2**) sebacic acid-modified; (**DA-ZrO_2**) dodecanedioic acid-modified; (**12AA-ZrO_2**) 12-amiododecanoic acid-modified; (**um-ZrO_2**) unmodified.

However, the spectrum of **12AA-ZrO_2** is very noteworthy because both amine and carboxyl groups in 12AA can attach to the surface through the coordination bond.[38]

The band around 3500 cm^{-1} indicates the stretching (ν N–H) mode of free amine ($-NH_2$).[37] The band between 1640 and 1560 cm^{-1} indicates the bending (δ N–H) mode of $-NH_2$. The band around 3000 cm^{-1} indicates the ν N–H mode of saturated amine ($-NH_3^+$), which depends on the counter anions. The δ_{as} and δ_s N–H modes of the $-NH_3^+$ are indicated between 1600 and 1575 cm^{-1}, and at 1500 cm^{-1}, respectively. These bending modes shift to high wavenumber with the intermolecular interaction such as hydrogen bond. Based on these band assignments, the original 12AA was identified (Fig. S1d†). The band at 3191 cm^{-1} is assigned to the ν N–H mode of amine groups. The bands at 1645 and 1515 cm^{-1} are assigned to the δ_{as} and δ_s N–H modes of amine groups, respectively. The band at 2121 cm^{-1} is assigned to the overtone band of $-NH_3^+$. The shoulder band around 1530 cm^{-1} and the band at 1393 cm^{-1} are assigned to the ν_{as} and ν_s modes of $-COO^-$, respectively. These results suggest that the original 12AA before treatment with SCW is in a zwitterionic ($-NH_3^+$ and $-COO^-$) state like amino acids. On the other hand, **12AA-ZrO_2** showed bands at 3310 and 1638 cm^{-1}, which are assigned to the ν N–H and the δ N–H modes of free amine ($-NH_2$), respectively. The stretching mode of the free carboxyl group (–COOH) was not observed in this case. Therefore, these results suggest that the carboxyl group in 12AA is certainly coordinated to the Zr ion at the surface of the ZrO_2 nanoparticles rather than the amine group, and thus free amine group is displayed at the surface. However, inspection of the spectrum of **12AA-ZrO_2** showed a weak band around 3080 cm^{-1}. This band suggests the ν N–H mode of the amide group.[37] The band of the amide group indeed overlaps that of the amine groups.[37] This result suggests that original 12AA is converted to other molecules *via* amide bond between amine and carboxyl groups under the hydrothermal conditions.

The FT-IR results suggest that under sub- or supercritical hydrothermal conditions, the reaction of amino acids or aminocarboxylic acids like 12AA proceeds in a manner in which these molecules are converted to dimer and/or easily cyclized *via* amide bond due to dehydration–oligomerization reaction in SCW.[39,40] Hence, the surface of **12AA-ZrO_2** contains not only 12AA monomer, but also its dimer or oligomer. In addition, the band intensity of $-CH_2-$ modes in the spectrum of **12AA-ZrO_2** was stronger than other surface-modified products. This is because the ratio of the $-CH_2-$ part to one molecule increases by the polymerization such as dimerization and oligomerization of 12AA. In any event, the free amine group originated in 12AA is displayed at the surface of **12AA-ZrO_2**.

These FT-IR observations showed that the surface modifiers with carboxyl group were attached to the surface of the ZrO_2 nanoparticles through the coordination bond between the carboxylate group ($-COO^-$) and the Zr ion. However, the FT-IR results could not provide any quantitative information about the amount of the attached surface modifiers on the nanoparticles. These results revealed that it is possible to attach the organic surface modifiers to ZrO_2 by using the supercritical hydrothermal method. Furthermore, the particle sizes of the surface-modified nanoparticles decreased by the surface modification.

(3) TGA measurements

To verify the coordination (chemical) bond and quantitatively estimate the amount of surface modifiers present on the nanoparticles, thermogravimetric analysis (TGA) was performed. Fig. 4 shows the TGA curves of the products. The TGA curves of all the surface-modified ZrO_2 nanoparticles showed a distinctive weight loss above 300 °C, which indicates the coordination bond between organic molecules and the surface of the nanoparticles.[26,27] The weight loss also indicates the amount of surface modifiers attached on the nanoparticles.[26,27] The **um-ZrO_2** also showed a slight weight loss in the measurement range; the weight loss is believed to be possibly due to the chemisorbed water. These results are consistent with the FT-IR results. However, the weight loss of **12AA-ZrO_2**, as indicated by the TGA curve, seems to continue and did not attain any plateau even up to 800 °C. This suggests incomplete combustion of the organic molecules in the measurement range.

The number of surface modifiers attached to one ZrO_2 nanoparticle was estimated using the weight loss at 800 °C. Correction was made for the weight loss (2.51%) in **um-ZrO_2** when

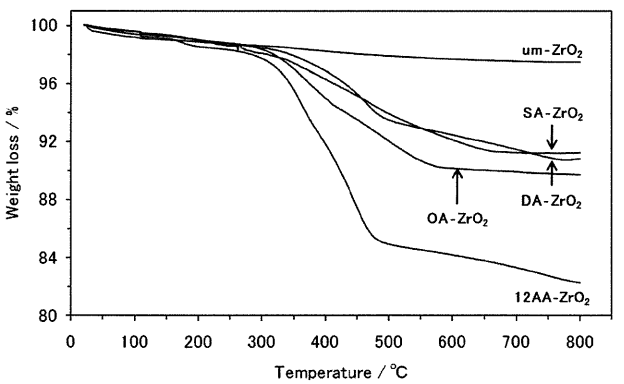

Fig. 4 TGA curves of the products: (**OA-ZrO_2**) oleic acid-modified; (**SA-ZrO_2**) sebacic acid-modified; (**DA-ZrO_2**) dodecanedioic acid-modified; (**12AA-ZrO_2**) 12-amiododecanoic acid-modified; (**um-ZrO_2**) unmodified.

estimating the weight loss of the surface-modified ZrO_2 nanoparticles. Although the combustion of the organic molecules in **12AA-ZrO_2** was not completed at 800 °C yet, we estimated the number of the attached molecules with a view to have a tentative idea about their attachment to the surface. The estimated values are summarized in Table 2. The number of the surface modifiers attached to the surface was about the same among **OA-**, **SA-**, and **DA-ZrO_2**. However, the number of attached 12AA in **12AA-ZrO_2** was four to eight times higher than the corresponding organic molecules attached to other surface modified nanoparticles (**OA-**, **SA-**, and **DA-ZrO_2**). The higher amount of attached 12AA is attributed to the formation of dimer and/or oligomer on the surface of **12AA-ZrO_2**. Fig. 5 shows a schematic illustration of the structure of the respective carboxylic acid-modified ZrO_2 nanoparticles.

(4) Zeta potential measurements

The surface properties of **SA-**, **DA-**, **12AA-**, and **um-ZrO_2** in water were investigated by measuring the pH dependence of their zeta potential. The zeta potential was estimated from the mobility of the colloidal particles in a suspension under the influence of an electric field. Zeta potential of **OA-ZrO_2** was not measured because it was not dispersed in water. The dispersibility of the nanoparticles in water depends on the functional groups at the surface. From the FT-IR results, the methyl

Table 2 TGA determination of the number of surface organic modifiers that attached to one surface-modified ZrO_2 nanoparticle

Products	Weight loss (%) from TGA	Coverage of modifier/ molecule nm^{-2}	Calculated number of modifiers that attached to one ZrO_2 nanoparticle
OA-ZrO_2	7.80	2.61	1961
SA-ZrO_2	6.26	2.21	1003
DA-ZrO_2	6.70	2.32	1313
12AA-ZrO_2	15.2	8.34	8390

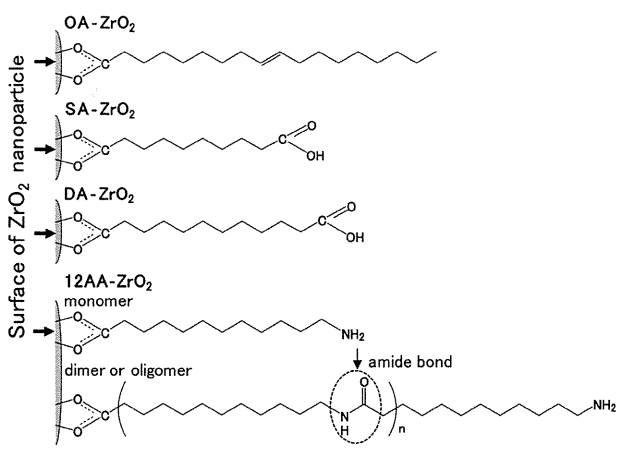

Fig. 5 Schematic illustration of the structure of the respective carboxylic acid-modified ZrO_2 nanoparticles: (**OA-ZrO_2**) oleic acid-modified; (**SA-ZrO_2**) sebacic acid-modified; (**DA-ZrO_2**) dodecanedioic acid-modified; (**12AA-ZrO_2**) 12-amiododecanoic acid-modified.

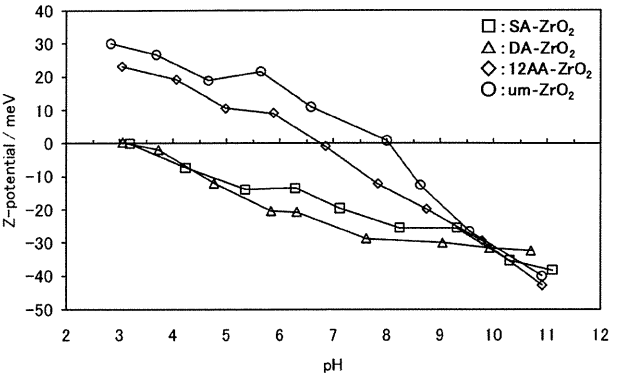

Fig. 6 Zeta potentials of the products: (□, **SA-ZrO_2**) sebacic acid-modified; (△, **DA-ZrO_2**) dodecanedioic acid-modified; (◇, **12AA-ZrO_2**) 12-amiododecanoic acid-modified; and (○, **um-ZrO_2**) unmodified at various pH values.

($-CH_3$) group displayed on the surface of **OA-ZrO_2** is a hydrophobic group.[41,42] Since the affinity of the hydrophobic group to water is low, **OA-ZrO_2** was not dispersed easily in water. On the other hand, carboxyl (–COOH), amine ($-NH_2$), and hydroxyl (–OH) groups, displayed on the surface of **SA-** (and **DA-**), **12AA-**, and **um-ZrO_2**, respectively, being hydrophilic in nature were easily dispersed in water.[41,42]

In this measurement, an important property is the isoelectric point (IEP), which is defined as the pH at which the particle has a net zero surface charge.[26,27] The IEP value depends on the charging mechanisms on the surface of the nanoparticles; therefore, it is expected to change with the surface modification. Fig. 6 shows the zeta potentials of the nanoparticles dispersed in water. The IEP value of **um-ZrO_2** is at pH 8.1, which changes significantly for surface-modified ZrO_2. The IEP of **SA-** and **DA-ZrO_2** was at pH 3.0. The low IEP values were due to the strongly acidic nature of the carboxyl group that was displayed at the surface of the nanoparticles.[26,27] The **12AA-ZrO_2** exhibited IEP value at pH 6.8, which is slightly higher than but close to the IEP values (*i.e.*, pH 6.0) of amino acids such as glycine or alanine with carboxyl and amine groups in the molecule one-by-one.[42] The higher IEP of **12AA-ZrO_2** suggests that the acidic nature of the carboxyl group of 12AA in **12AA-ZrO_2** is weak due to the coordination bond between the carboxylate group ($-COO^-$) and the Zr ion. These results suggest that the attached modifiers at the surface of the ZrO_2 nanoparticles remained in water and the functional groups, such as carboxyl and amine, are displayed at the surface of the ZrO_2 nanoparticles, which is consistent with the FT-IR results.

Conclusion

This study succeeded in rapid and simple synthesis of surface-modified monoclinic ZrO_2 nanoparticles from $Zr(OH)_4$ in the presence of various surface modifiers with carboxyl group using the supercritical hydrothermal method. The surface modifiers were attached to the surface of the nanoparticles through the coordination bond between the carboxylate group and the Zr ion. The particle size of the surface-modified nanoparticles was smaller than that of the unmodified one. This reduction in particle size is attributed to the inhibition of the growing surface

of the nanoparticles due to surface modification. The surface-modified nanoparticles displayed functional groups, such as methyl, carboxyl, and amine, at the surface. Sebacic, dodecanedioic, and 12-aminododecanoic acid-modified ZrO_2 nanoparticles were dispersed in water due to the functional groups at the surface. The IEP values of ZrO_2 nanoparticles depended on the nature of their functional groups. The particle size of monoclinic ZrO_2 nanoparticles could be reduced by surface modification during the supercritical hydrothermal method, thereby demonstrating the effectiveness of this method for synthesizing the nanoparticles.

Acknowledgements

This work was supported by a Grant-in-Aid for Scientific Research (S) (KAKENHI) no. 20226015.

References

1 A. P. Alivisatos, *Science*, 1996, **271**, 933–937.
2 M. V. Kovalenko, M. I. Bodnarchuk, R. T. Lechner, G. Hesser, F. Schäffler and W. Heiss, *J. Am. Chem. Soc.*, 2007, **129**, 6352–6353.
3 I. L. Medintz, H. T. Uyeda, E. R. Goldman and H. Mattoussi, *Nat. Mater.*, 2005, **4**, 435–446.
4 S. Sun, H. Zeng, D. B. Robinson, S. Raoux, P. M. Rice, S. X. Wang and G. Li, *J. Am. Chem. Soc.*, 2004, **126**, 273–279.
5 T. Zhang, J. Ge, Y. Hu and Y. Yin, *Nano Lett.*, 2007, **7**, 3203–3207.
6 S. K. Smoukov, K. J. M. Bishop, B. Kowalczyk, A. M. Kalsin and B. A. Grzybowski, *J. Am. Chem. Soc.*, 2007, **129**, 15623–15630.
7 A. M. Kalsin, M. Fialkowski, M. Paszewski, S. K. Smoukov, K. J. M. Bishop and B. A. Grzybowski, *Science*, 2006, **312**, 420–424.
8 S. Chen, Y. Li, C. Guo, J. Wang, J. Ma, X. Liang, L.-R. Yang and H.-Z. Liu, *Langmuir*, 2007, **23**, 12669–12676.
9 M. Kasture, S. Singh, P. Patel, P. A. Joy, A. A. Prabhune, C. V. Ramana and B. L. V. Prasad, *Langmuir*, 2007, **23**, 11409–11412.
10 S. S. Banerjee and D.-H. Chen, *Chem. Mater.*, 2007, **19**, 6345–6349.
11 Z. Chen, H. Chen, H. Hu, M. Yu, F. Li, Q. Zhang, Z. Zhou, T. Yi and C. Huang, *J. Am. Chem. Soc.*, 2008, **130**, 3023–3029.
12 E. C. Subbarao, H. S. Maiti and K. K. Srivastava, *Phys. Status Solidi A*, 1974, **21**, 9–40.
13 M. Yashima, T. Kato, M. Kakihana, M. A. Gulgun, Y. Matsuo and M. Yoshimura, *J. Mater. Res.*, 1997, **12**, 2575–2583.
14 J. H. Shin, C.-C. Chao, H. Huang and F. B. Prinz, *Chem. Mater.*, 2007, **19**, 3850–3854.
15 R. C. Garvie, R. H. J. Hannink and R. T. Pascoe, *Nature*, 1975, **258**, 703–704.
16 J. W. Bae, J. Y. Park, S. W. Hwang, G. Y. Yeom, K. D. Kim, Y. A. Cho, J. S. Jeon and D. Choi, *J. Electrochem. Soc.*, 2000, **147**, 2380–2384.
17 L. Ouyang and W. Y. Ching, *J. Appl. Phys.*, 2004, **95**, 7918–7924.
18 D. He, Y. Ding, H. Luo and C. Li, *J. Mol. Catal. A: Chem.*, 2004, **208**, 267–271.
19 C.-M. Wang, K.-N. Fan and Z.-P. Liu, *J. Am. Chem. Soc.*, 2007, **129**, 2642–2647.
20 G. D. Wilk, R. M. Wallace and J. M. Anthony, *J. Appl. Phys.*, 2001, **89**, 5243–5275.
21 G. Wang, F. Meng, C. Ding, P. K. Chu and X. Liu, *Acta Biomater.*, 2010, **6**, 990–1000.
22 K. Sato, H. Abe and S. Ohara, *J. Am. Chem. Soc.*, 2010, **132**, 2538–2539.
23 H. Hayashi, A. Ueda, A. Suino, K. Hiro and Y. Hakuta, *J. Solid State Chem.*, 2009, **182**, 2985–2990.
24 N. Zhao, D. Pan, W. Nie and X. Ji, *J. Am. Chem. Soc.*, 2006, **128**, 10118–10124.
25 J. Joo, T. Yu, Y. W. Kim, H. M. Park, F. Wu, J. Z. Zhang and T. Hyeon, *J. Am. Chem. Soc.*, 2003, **125**, 6553–6557.
26 M. Taguchi, S. Takami, T. Naka and T. Adschiri, *Cryst. Growth Des.*, 2009, **9**, 5297–5303.
27 M. Taguchi, S. Takami, T. Adschiri, T. Nakane, K. Sato and T. Naka, *CrystEngComm*, 2011, **13**, 2841–2848.
28 S. Takami, S. Ohara, T. Adschiri, Y. Wakayama and T. Chikyow, *Dalton Trans.*, 2008, 5442–5446.
29 T. Mousavand, T. Naka, K. Sato, S. Ohara, M. Umetsu, S. Takami, T. Nakane, A. Matsushita and T. Adschiri, *Phys. Rev. B: Condens. Matter Mater. Phys.*, 2009, **79**, 144411.
30 M. Taguchi, S. Takami, T. Adschiri, T. Nakane, K. Sato and T. Naka, *CrystEngComm*, 2012, DOI: 10.1039/c2ce06408a.
31 Y. Arai, T. Sako, and Y. Takebayashi, *Supercritical Fluids*, Springer, Berlin, 2001.
32 Y.-P. Sun, *Supercritical Fluid Technology in Materials Science and Engineering*, Marcel Dekker, New York, 2002.
33 R. C. Garvie, *J. Phys. Chem.*, 1978, **82**, 218–224.
34 H. Toraya, M. Yoshimura and S. Somiya, *J. Am. Ceram. Soc.*, 1984, **67**, c119–c121.
35 H. Miura, *J. Crystallogr. Soc. Jpn.*, 2003, **45**, 145–147.
36 C. M. Phillippi and K. S. Mazdiyasni, *J. Am. Ceram. Soc.*, 1971, **54**, 254–259.
37 K. Nakanishi, *Infrared Absorption Spectroscopy: Practical*, Holden-Day, San Francisco, 1962.
38 K. Nakamoto, *Infrared and Raman Spectra of Inorganic and Coordination Compounds*, Wiley, New York, 1997.
39 M. N. Islam, T. Kaneko and K. Kobayashi, *Bull. Chem. Soc. Jpn.*, 2003, **76**, 1171–1178.
40 Y. Futamura, K. Yahara and K. Yamamoto, *J. Supercrit. Fluids*, 2007, **41**, 279–284.
41 J. N. Israelachivili, *Intermolecular and Surface Forces*, Academic Press, London, 1991.
42 H. Hart, *Organic Chemistry: A Short Course 8th Edition*, Houghton Mifflin Company, Boston, 1991.

J. of Supercritical Fluids 62 (2012) 190–196

Contents lists available at SciVerse ScienceDirect

The Journal of Supercritical Fluids

journal homepage: www.elsevier.com/locate/supflu

Synthesis of shape-controlled and organic-hybridized hafnium oxide nanoparticles under sub- and supercritical hydrothermal conditions

Ameneh Sahraneshin[a,b], Seiichi Takami[b], Daisuke Hojo[c], Kimitaka Minami[d], Toshihiko Arita[b], Tadafumi Adschiri[b,c,d,*]

[a] Graduate School of Engineering, Tohoku University, 6-6 Aramaki Aza Aoba, Aoba-ku, Sendai 980-8579, Japan
[b] Institute of Multidisciplinary Research for Advanced Materials, Tohoku University, 2-1-1 Katahira, Aoba-ku, Sendai 980-8577, Japan
[c] Advanced Institute for Materials Research (WPI-AIMR), World Premier International Research Center, Tohoku University, 2-1-1 Katahira, Aoba-ku, Sendai 980-8577, Japan
[d] New Industry Creation Hatchery Center, Tohoku University, 6-6-10 Aramaki Aza Aoba, Aoba-ku, Sendai 980-8579, Japan

ARTICLE INFO

Article history:
Received 29 June 2011
Received in revised form 24 October 2011
Accepted 31 October 2011

Keywords:
Hafnium oxide
Nanoparticles
Sub- and supercritical water
Surface modification

ABSTRACT

In this study, hafnium oxide nanoparticles with different sizes and morphologies were synthesized under sub- and supercritical hydrothermal conditions and with and without organic surface modifiers. Transmission electron microscopy images showed that various shapes such as trapezohedron, oval-like and irregular shaped particles with sizes from 8 to 20 nm were obtained depending on the reaction conditions. The synthesized particles had monoclinic crystal structures as evidenced by their X-ray diffraction patterns. Chemical bonding of organic surface modifiers and their density on the particle surfaces were evaluated by Fourier transform infrared spectroscopy and thermogravimetric analysis. Furthermore, the effects of sub- and supercritical water state as the reaction medium and the presence of organic surface modifiers with different functional groups on the size and morphology of the particles are discussed.

1. Introduction

A wide range of research and development has been conducted in the past decade on the synthesis of metal oxide nanoparticles (NPs) because they have applications in various fields including optics, semiconductors, catalysis, drug delivery, and bio-imaging [1–7]. Hafnium oxide (hafnia, HfO_2) is an important ceramic material because of its large dielectric constant (~30), high melting point (2758 °C), and chemical stability. HfO_2 and its solid solution with SiO_2 are highly promising replacements for SiO_2 as gate dielectrics in metal-oxide-semiconductor devices because they can increase the film thickness and reduce the leakage current [8,9]. Because HfO_2 has a high dielectric constant, relatively low leakage current, large band gap (5.68 eV), and high transparency, it can be used in the liquid crystal (LC) alignment process to increase the capacitance of the inorganic alignment layer for the low-voltage driving of LCs [10]. Because of its high refractive index (~2.9), hafnia is expected to be a good candidate to be dispersed in photoresist polymers or immersion liquids to improve their refractive index and reach higher resolutions for recently developed immersion lithography techniques [11–13]. However, optical transparency dictates the use of extremely small NPs in order to avoid excessive light scattering. Furthermore, uniform dispersion of NPs in the matrix is the key factor for the successful fabrication of a transparent, uniform organic–inorganic nanocomposite.

To date, hafnium oxide NPs have been synthesized via various procedures including the sol–gel, solvothermal, hydrothermal, microwave–hydrothermal methods [14–17]. The size, morphology, and surface characteristics of NPs strongly affect their optical, electrical, catalytic, and other physical properties [18,19]; therefore, it is crucial to consider the required specifications of the target NPs before choosing the synthesis method. Furthermore, to commercialize a lab-scale synthesis method to the industrial scale, it is important to design an ecologically benign process. However, a generalized method for the synthesis of shape- and size-controlled hafnia NPs considering the ecological aspects has not yet been developed.

Supercritical hydrothermal techniques, in which supercritical water is the reaction medium, have been studied as a promising green method to synthesize metal oxide NPs with narrow size distributions [20,21]. In the present study, we synthesized hafnium oxide NPs with uniform size distributions under supercritical hydrothermal conditions. We also tried to control the size, morphology, and surface properties of the hafnia NPs for the first time by using different types of organic surface modifiers (carboxylic acids, aldehydes, and amines) via a process of in situ synthesis and surface modification. The dielectric constant of supercritical water is close to that of polar organic solvents (10–20) and provides miscibility with organic modifiers that can

* Corresponding author at: WPI-AIMR, Tohoku University, 2-1-1 Katahira, Aoba-ku, Sendai 980-8577, Japan. Tel.: +81 22 217 6321; fax: +81 22 217 6321.
E-mail address: ajiri@tagen.tohoku.ac.jp (T. Adschiri).

0896-8446/$ – see front matter © 2011 Elsevier B.V. All rights reserved.
doi:10.1016/j.supflu.2011.10.019

bind to the nanoparticle's surface and modify the particle's surface chemical character [22].

2. Materials and methods

2.1. Preparation of precursor solutions

The starting materials were hafnium tetrachloride, $HfCl_4$ [99.99%, Wako Chemicals] and potassium hydroxide, KOH [99.99%, Wako Chemicals]. The precursor solution was prepared by dissolving hafnium tetrachloride (0.160 g) in deionized water (10.0 mL). Potassium hydroxide solution (0.20 M, 10.0 mL) was added drop-wise to the precursor solution under continuous stirring, to convert hafnium tetrachloride to hafnium hydroxide [23,24] as shown in the following reactions:

$$HfCl_4 + 2H_2O \rightarrow Hf(OH)_2Cl_2 + 2HCl$$

$$Hf(OH)_2Cl_2 + 2KOH \rightarrow Hf(OH)_4 + 2KCl$$

The white slurry solution was washed with deionized water to remove all K^+ and Cl^- ions in two cycles of centrifugation–decantation. The precipitate was then dispersed in 10.0 mL of deionized water.

2.2. Synthesis of hafnium oxide NPs

The precursor solution (2.5 mL) was loaded into a pressure-resistant tube reactor (SUS 316) whose inner volume was 5.0 mL. For the synthesis of the surface modified NPs, 7.5×10^{-4} mol of the respective organic modifier (decylamine, decanal, or decanoic acid) was added. The molar ratio of hafnium ions to organic reagents was 1:6. All organic reagents were purchased from Wako Chemicals. The reactors were then capped tightly and put in an electric furnace whose temperature was set beforehand. When we set the temperature of the furnace to 350 °C and 400 °C, the temperature inside the reactor reached to 335 °C and 395 °C, respectively. The reaction was stopped after 10 min by quenching the reactor in a water bath at room temperature. The reaction products, which were whitish aqueous mixtures of synthesized NPs and unreacted modifiers, were collected by 3 mL of hexane. The mixture was strongly shaken and kept for 1 h to separate the organic and aqueous phases. The aqueous phase was removed and the remaining solution was washed using ethanol in three cycles of centrifugation and decantation to remove unreacted organic molecules. Finally, the particles were dispersed in cyclohexane and freeze-dried under vacuum for 6 h. For the unmodified NPs, the products were washed using deionized water in two cycles of centrifugation and decantation, and then dispersed in water and freeze-dried under vacuum overnight.

2.3. Characterization

The crystallinity and purity of the particles were identified using an X-ray diffractometer (XRD, Rigaku Ultima IV) with Cu Kα radiation in a 2θ–θ setup. The 2θ angle was scanned between 15° and 80°. The size and morphology of the particles were analyzed using transmission electron microscopy (TEM, Hitachi H7650) at an accelerating voltage of 100 kV. Fourier transform infrared (FTIR) spectra were acquired using a JASCO FT/IR-680 spectrometer to investigate the chemical bonding and functional groups on the particle surfaces. The transmission IR spectra were collected from 400 to 4000 cm^{-1}. The density of organic molecules attached on the particles was estimated by thermogravimetric analysis (TGA), conducted under a constant flow of Ar gas, in the temperature range 20–800 °C with a ramp rate of 10 °C/min.

3. Results

3.1. Effect of temperature on the synthesis of hafnium oxide NPs in the absence of organic capping agents

Hafnium oxide NPs were synthesized at different sub- to supercritical temperatures of water (250, 300, 350, and 400 °C) in the absence of organic capping agents. Fig. 1 shows the XRD patterns of the synthesized NPs. No hafnium hydroxide NPs crystallized at 250 °C; however, at 300, 350, and 400 °C, the XRD patterns showed good crystallization of the products. Comparing the XRD patterns of the NPs to the Joint Committee on Powder Diffraction Standards (JCPDS) patterns of different crystal phases of hafnium oxide (monoclinic, orthorhombic, and tetragonal) we determined that the obtained NPs had a monoclinic structure.

The TEM images, shown in Fig. 2, reveal that the shapes of the particles synthesized in subcritical temperatures of water (Fig. 2b and c) are different from those synthesized in supercritical water (Fig. 2d). From the magnified and high resolution TEM images (Fig. 2e and f) it can be seen that the particles formed 16-nm-sized trapezohedron structures under subcritical conditions (300 and 350 °C). Interestingly, when the temperature rose to the supercritical temperature of water (400 °C), the particle shapes changed to oval-like (Fig. 2d) but remained the same size.

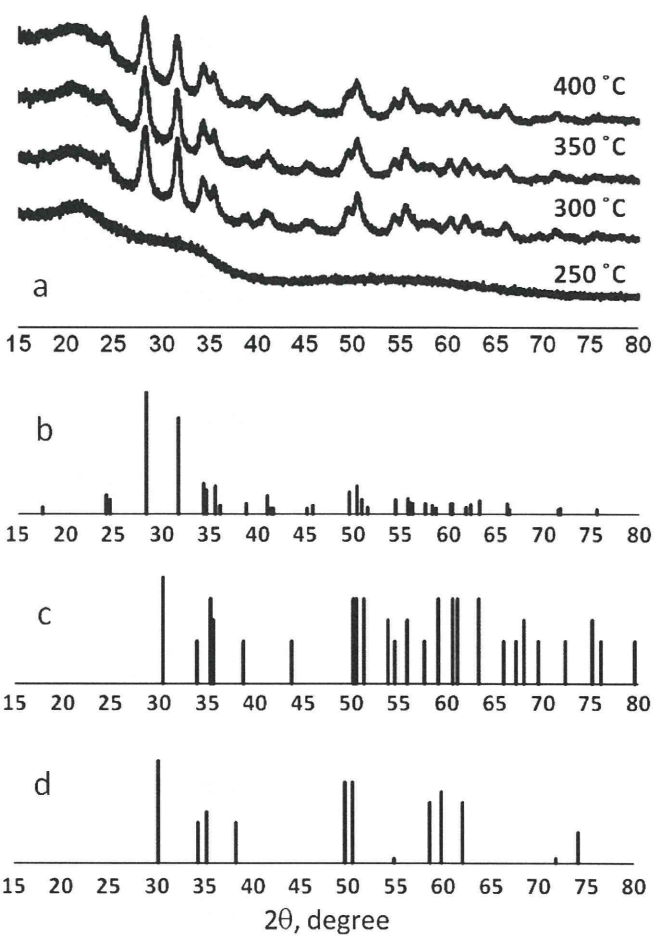

Fig. 1. (a) XRD pattern of the synthesized HfO_2 NPs at different temperatures; (b–d) JCPDS patterns of monoclinic (b), orthorhombic (c) and tetragonal (d) HfO_2 (JCPDS codes: 34-0104, 21-0904, and 08-0342 respectively).

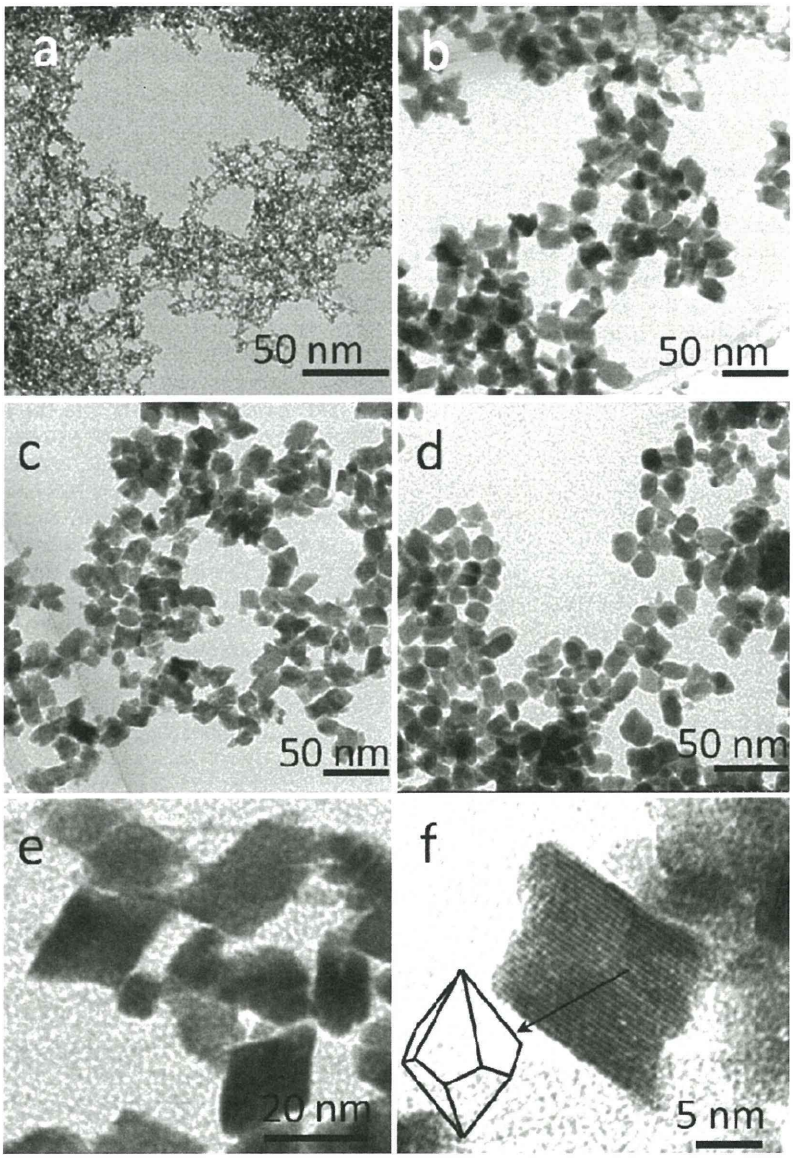

Fig. 2. TEM (a–e) and HRTEM (f) images of the synthesized HfO_2 NPs at (a) 250 °C, (b) 300 °C, (c–f) 350 °C, and (d) 400 °C.

3.2. *Effect of organic surface modifiers on the morphology of particles*

Fig. 3 depicts the XRD patterns of HfO_2 NPs synthesized in the presence of different organic capping agents at 350 and 400 °C. In the presence of organic modifiers, the NP crystal phase is still monoclinic. The XRD peaks in the decanoic acid-modified NPs are broader and less sharp compared with the peaks for the decylamine- and decanal-modified NPs. This indicates that the decanoic acid-modified NPs are smaller and less crystallized compared with the other two modified NPs. To investigate this, the particle sizes were estimated from Scherrer's correlation using the following equation:

$$D = \frac{K\lambda}{\beta \cos\theta} \quad (1)$$

where K is the dimensionless shape factor (typically 0.89), λ is the X-ray wavelength (0.154 nm), β is the line broadening at half the maximum intensity in radians, and θ is the Bragg angle. The estimated values for the particle sizes, summarized in Table 1, show that the decanoic acid-modified NPs are smaller compared with the other two modified NPs.

From the TEM images in Fig. 4 the particles synthesized under supercritical conditions (400 °C) have clearer image and more marked sign compared to those produced in subcritical conditions (350 °C), in the presence of all modifiers. The decylamine-modified particles are irregular in shape with average size of about 20 nm and the decanal-modified particles are similar in size and shape to the unmodified NPs (cf. Fig. 2c and d). From the TEM image in Fig. 4e, the decanoic acid-modified NPs show a drastic change in shape and size under subcritical conditions. Under supercritical conditions (Fig. 4f), the decanoic acid-modified NP sizes are reduced to 11 nm, and the shape remains oval-like, similar to the unmodified NPs. The NPs sizes from the TEM images and those calculated from Scherrer's equation are in good agreement and indicate that single crystalline NPs were formed in all cases.

Table 1
Particle sizes estimated from Scherrer's equation and TEM images.

Temperature [°C]	Modifier/size (nm)							
	Without modifier		Decylamine		Decanoic acid		Decanal	
	TEM	XRD	TEM	XRD	TEM	XRD	TEM	XRD
350	16	16.2	20	19.1	–	13.6	16	16.9
400	16	15.3	20	17.8	11	11.4	16	16.4

3.3. Surface properties of the particles

3.3.1. Chemical bonding on the particle surfaces

To verify the existence of organic modifiers chemically bonded on the particle surfaces, the FTIR spectra of the synthesized particles and neat modifiers were measured, as shown in Fig. 5. New peaks in the region 2800–2960 cm^{-1} appear in the spectra of the surface-modified NPs compared with the unmodified NP spectra. These peaks are assigned to the C–H stretching mode of the methyl and methylene groups, and are present in the FTIR spectra of the neat modifiers, indicating the existence of organic molecules on the NP surfaces. In the spectra of the decanoic acid-modified NPs, the two major peaks at 1534 and 1440 cm^{-1} are assigned to the asymmetric and symmetric modes, respectively, of the carboxyl group [22] and indicate that the decanoic acid is chemically bonded to the HfO_2 NP surface by its carboxyl group. In contrast, there was no observable peak at around 1600 cm^{-1} in the decylamine modified NP spectra to indicate the chemical bonding via the amino ($-NH_2$) [25]. We surmise that this modifier could not make strong chemical bonds on the surface of HfO_2 particles during the hydrothermal reaction. In the spectra of decanal modified NPs also there is not any visible band at around 1700 cm^{-1} to show the chemical bonding of carbonyl group on the NP surface [26]. On the other hand, very less intense peaks are observable at around 1534 and 1440 cm^{-1}. As mentioned in previous sentences, these peaks are attributed to the chemical bonding of carboxylic acid. This indicates that under the reaction conditions, aldehyde group oxidized to carboxyl group. However it seems that the oxidation was not that much to control the NP shapes as perfect as direct addition of decanoic acid into the reaction mixture.

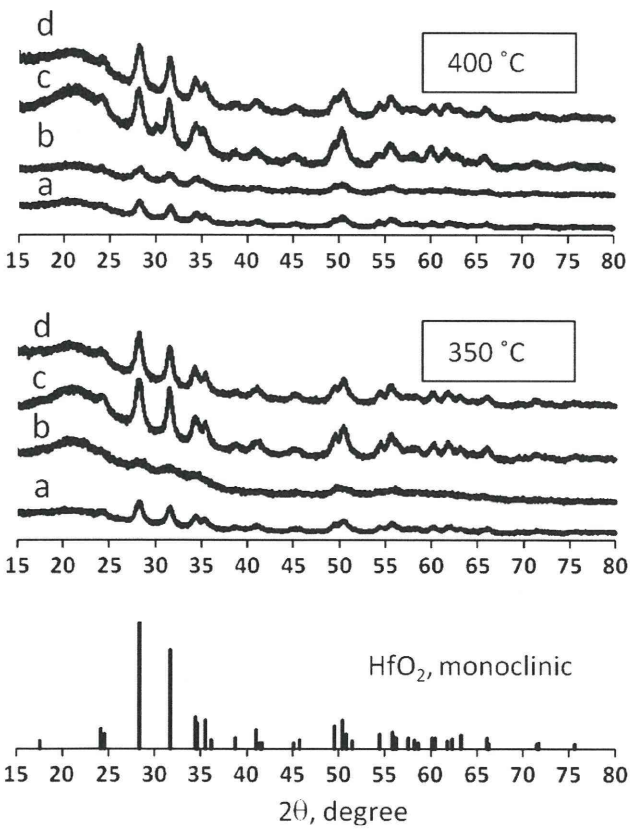

Fig. 3. XRD pattern of the synthesized NPs in the presence of (a) decylamine, (b) decanoic acid, (c) decanal, and (d) in the absence of organic modifiers (Standard pattern shows the JCPDS [34-0104] pattern, monoclinic HfO_2).

3.3.2. Density of modifiers on the particle surfaces

The amount of organic modifiers attached on the NP surfaces was estimated using thermogravimetric analysis (TGA) in the temperature range 20–800 °C. Fig. 6 shows that under both sub- and supercritical conditions an extra weight loss occurs between 270 and 550 °C for the surface-modified NPs compared to the unmodified NPs. This weight loss is due to the decomposition and calcinations of organic surface modifiers from the NP surface by increasing the temperature up to their boiling points (decanoic acid: 269 °C, decanal: 208 °C and decylamine: 217 °C) which provides more evidence for the existence of organic surface modifiers on the surface of synthesized HfO_2 NPs. The amounts of weight losses for different surface modifiers are summarized in Table 2, and it is observed that the largest weight lost occurs for the decanoic acid-modified NPs. This reliably confirms the TEM, XRD, and FTIR results indicating the effective role of this capping agent in binding to HfO_2 NPs and controlling the NP growth during the hydrothermal reaction.

It is also worth mentioning that the weight loss in the temperature range 20–800 °C for all particles corresponds to the desorption of the remaining water molecules from the hydrothermal reaction and also re-crystallization of the un-reacted amorphous precursor in the samples. To investigate the amount of amorphous phase in the products the TGA curve of the amorphous product that synthesized at 250 °C is compared with the TGA curves of the particles synthesized at 350 °C and 400 °C. Results are shown in Fig. 7. TGA curves show 14.35%, 3.49% and 4.08% weight loss for the samples synthesized at 250 °C, 350 °C and 400 °C, respectively, which are corresponding to the crystallization of amorphous phase and decomposition of water molecules from the samples. Comparing the weight losses, it can be concluded that there is not a significant amount of amorphous phase in the products obtained at 350 °C and 400 °C.

Table 2
Weight losses (%) of different surface modifiers under sub- and supercritical conditions.

Temperature [°C]	Modifier		
	Decylamine	Decanoic acid	Decanal
350	3.2	12.9	4.8
400	3.1	7.9	4.1

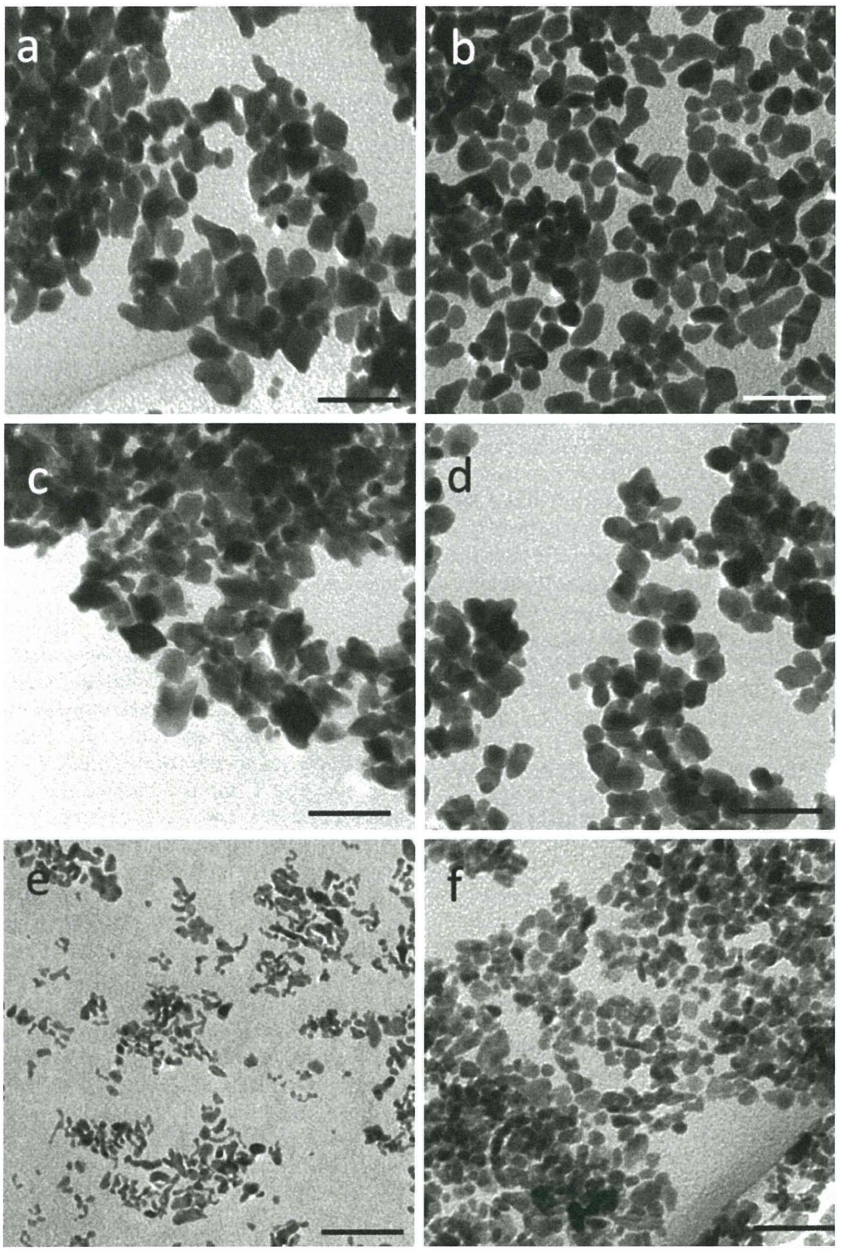

Fig. 4. TEM images of the synthesized NPs at 350 °C (a, c, and e) and 400 °C (b, d, and f), in the presence of decylamine (a and b), decanal (c and d), and decanoic acid (e and f). Scale bars: 50 nm.

4. Discussion

The size and shape of NPs synthesized under sub- and supercritical conditions are significantly influenced by the properties of the reaction media. The crystallization of NPs involves the precipitation of a solid phase from solution, which consists of a nucleation step followed by crystal growth. Upon changing the medium from the subcritical to the supercritical phase, the degree of supersaturation increases and therefore the nucleation rate increases [27], leading to the formation of smaller sized NPs. The synthesis of smaller sized NPs using supercritical water has been the focus of many research groups [4,28,29]. However, based on our experimental results, we believe that the drastic change in properties of water in the supercritical state can also affect the NP growth behavior. As well as increasing the nucleation rate, the growth rate of the crystallographic planes also changes under supercritical conditions; crystallographic planes that could not grow uniformly under subcritical conditions begin to develop spherical surfaces under supercritical conditions. This also occurs in the presence of organic modifiers, as the NPs synthesized under supercritical conditions had clearer image and more marked sing compared to those obtained under subcritical conditions.

Addition of organic surface modifiers in the reaction mixture can hinder crystal growth. Amine molecules usually act as shape-determining agents and control the nanocrystal growth in such a preferential manner to ensure the formation of anisotropic nanostructures [30,31]. In this study, we surmise that decylamine most probably disturbed the growth of the nanocrystals leading to the formation of irregular-shaped structures. It has been already reported that carboxylic acids have a high tendency to hybridize

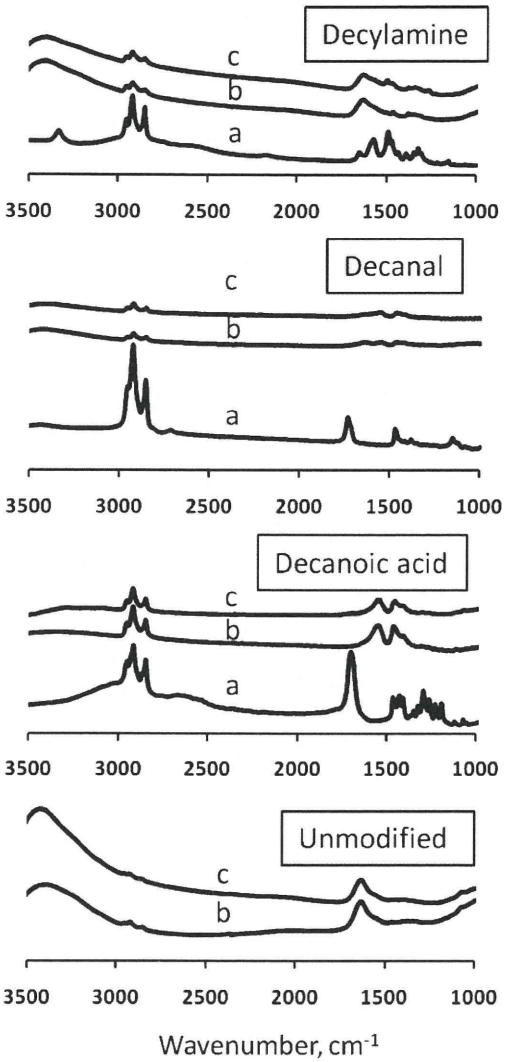

Fig. 5. FTIR spectra of: (a) neat modifier, (b) particles synthesized at 350 °C, and (c) particles synthesized at 400 °C.

with NPs via the carboxyl group and for controlling NP sizes and morphologies [21,29,32]. In our case, decanoic acid could successfully control the size of HfO_2 NPs by bonding to the NP surface through its COO^- group. Based on the FTIR results, some of the decanal molecules oxidized to decanoic acid under the reaction conditions. However existence of very weak FTIR peaks reveals that only a few organic molecules could attach on the surface of NPs. This is the reason why no significant change occurred in the NP size and morphology in the presence of decanal.

The average particle sizes estimated from Scherrer's equation against the amount of modifier weight losses from the TGA data are plotted in Fig. 8. There is an inverse relationship between these two parameters, i.e., increasing the amount of modifier molecules on the NP surfaces leads to the formation of NPs with smaller sizes. This result provides further evidence for the ability of decanoic acid molecules to control the NP's size compared to decylamine and decanal.

Due to its high refractive index (RI = 2.9), recently hafnia NPs has been proposed as a good candidate to be dispersed in polymeric matrices and fabrication of high refractive index nanocomposites. However the compatibility of NP surface with the polymer is a keen issue to achieve uniform dispersion of NPs in the matrix.

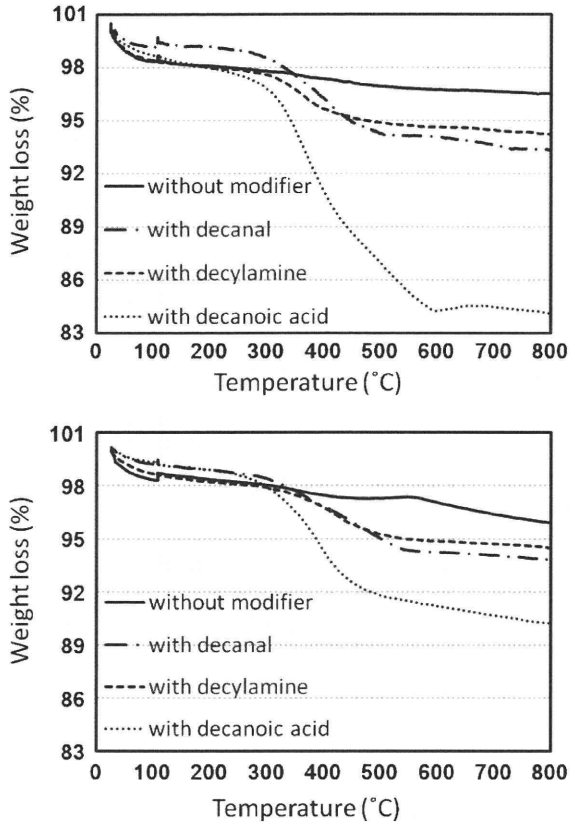

Fig. 6. TGA curves of the synthesized NPs at 350 °C (upper curve) and 400 °C (lower curve).

The hydrophobic surface character of synthesized NPs due to the attachment of carboxylic acids helps the particles to be dispersed in polymers easier. However the optical transparency is also a very delicate issue in this concern. In fact, carboxylic acids are not optically transparent and may defect the transparency of NPs. As the next step of the research we are trying to synthesize surface modified hafnium oxide NPs by using other organic molecules with less light absorptions. Phosphonic acids are the first candidates for this purpose.

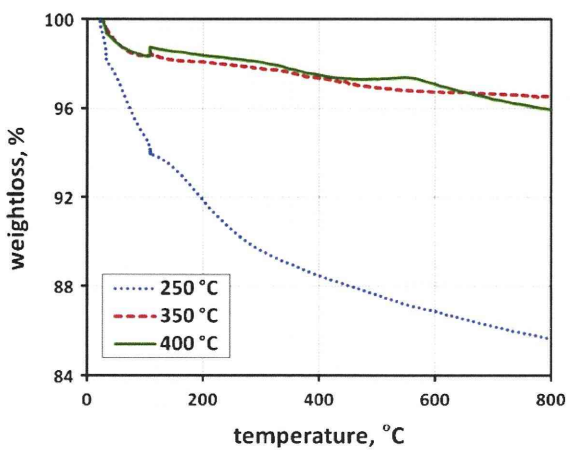

Fig. 7. TGA curves of the samples synthesized in the absence of surface modifiers at different temperatures.

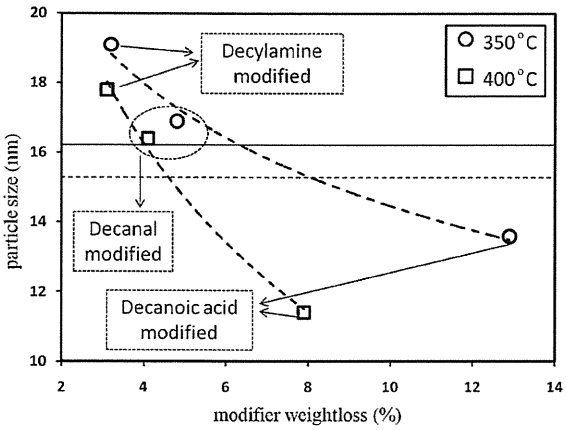

Fig. 8. Relationship between the modifiers weightloss and NP size. Horizontal lines show the mean size of unmodified particles at 350 °C (solid) and 400 °C (dashed).

5. Conclusions

In the present study, pure monoclinic phase hafnium oxide NPs were synthesized at sub- and supercritical temperatures of water using a simple rapid hydrothermal synthesis route with 10-min reaction time. Under subcritical conditions (300 and 350 °C), trapezohedron-shaped particles were synthesized, and under supercritical conditions (400 °C), the particle shapes changed to oval-like. In both cases NP sizes were around 16 nm. The possibility of controlling the particle size and surface properties were also investigated using organic surface modifiers. In the presence of decylamine, irregular-shaped HfO_2 NPs were formed. Decanal, an aldehyde, did not have any effect on the particle size and morphology. However, in the presence of decanoic acid the NP size drastically reduced. In the presence of all organic reagents, under supercritical conditions the NP's shape and crystal structure were more developed compared to subcritical conditions and all surface-modified particles showed hydrophobic surface characteristics.

Acknowledgement

The authors gratefully acknowledge Mr. Takamichi Miyazaki for obtaining the high-resolution TEM results.

References

[1] J.D. Holmes, D.M. Lyons, K.J. Ziegler, Supercritical fluid synthesis of metal and semiconductor nanomaterials, Chemistry European J. 9 (2003) 2144–2150.
[2] D. Rangappa, S. Ohara, M. Umetsu, T. Naka, T. Adschiri, Synthesis, characterization and organic modification of copper manganese oxide nanocrystals under supercritical water, J. Supercritical Fluids 44 (2008) 441–445.
[3] T. Adschiri, Supercritical hydrothermal synthesis of organic–inorganic hybrid nanoparticles, Chemistry Letters 36 (2007) 1188–1193.
[4] S. Kawasaki, Y. Xiuyi, K. Sue, Y. Hakuta, A. Suzuki, K. Arai, Continuous supercritical hydrothermal synthesis of controlled size and highly crystalline anatase TiO_2 nanoparticles, J. Supercritical Fluids 50 (2009) 276–282.
[5] S.T. Chang, S.H. Liao, Light emission and photoluminescence from high-k dielectrics containing Ge nanocrystals, J. Vacuum Science and Technology B 27 (2009) 535–537.
[6] P.R. Gil, D. Huhn, L.L. Mercato, D. Sasse, W.J. Parak, Nanopharmacy: inorganic nanoscale devices as vectors and active compounds, Pharmacological Research 62 (2010) 115–125.
[7] V.I. Shubayev, T.R. Pisanic, S. Jin, Magnetic nanoparticles for theragnostics, Advanced Drug Delivery Reviews 61 (2009) 467–477.
[8] G.D. Wilk, R.M. Wallace, J.M. Anthony, High-k gate dielectrics: current status and materials properties considerations, J. Applied Physics 89 (2001) 5243–5275.
[9] A.A. Rastorguev, V.I. Belyi, T.P. Smirnova, L.V. Yakovkina, M.V. Zamoryanskaya, V.A. Gritsenko, H. Wong, Luminescence of intrinsic and extrinsic defects in hafnium oxide films, Physical Review B 76 (2007) 235315.
[10] W.K. Lee, B.Y. Oh, J.H. Lim, H. Park, B.Y. Kim, H.J. Na, D.S. Seo, Vertical alignment of liquid crystals on a fully oxidized HfO_2 surface by ion bombardment, Applied Physics Letters 94 (2009) 223507.
[11] L. Bremer, R. Tuinier, S. Jahromi, High refractive index nanocomposite fluids for immersion lithography, Langmuir 25 (2009) 2390–2401.
[12] P.A. Zimmerman, B.J. Rice, E.C. Piscani, V. Liberman, High index 193 nm immersion lithography: the beginning or the end of the road, Proceedings of SPIE: The International Society for Optical Engineering 7274 (2009) 727420.
[13] W.J. Bae, M. Trikeriotis, J. Sha, E.L. Schwartz, R. Rodriguez, P. Zimmerman, E.P. Giannelis, C.K. Ober, High refractive index and high transparency HfO_2 nanocomposites for next generation lithography, J. Materials Chemistry 20 (2010) 5186–5189.
[14] P.E. Meskin, A.I. Gavrilov, V.D. Maksimov, V.K. Ivanov, B.P. Churagulov, Hydrothermal/microwave and hydrothermal/ultrasonic synthesis of nanocrystalline titania, zirconia and hafnia, Russian J. Inorganic Chemistry 52 (2007) 1648–1656.
[15] P.E. Meskin, F.Y. Sharikovb, V.K. Ivanov, B.R. Churagulov, Y.D. Tretyakov, Rapid formation of nanocrystalline HfO_2 powders from amorphous hafnium hydroxide under ultrasonically assisted hydrothermal treatment, Materials Chemistry and Physics 104 (2007) 439–443.
[16] A. Pucci, G. Clavel, M.G. Willinger, D. Zitoun, N. Pinna, Transition metal-doped ZrO_2 and HfO_2 nanocrystals, J. Physical Chemistry C 113 (2009) 12048–12058.
[17] J. Buha, D. Arčon, M. Niederberger, I. Djerdj, Solvothermal and surfactant-free synthesis of crystalline Nb_2O_5, Ta_2O_5, HfO_2, and co-doped HfO_2 nanoparticles, Physical Chemistry Chemical Physics 12 (2010) 15537–15543.
[18] W.E Buhro, V.L. Colvin, Semiconductor nanocrystals: shape matters, Nature Materials 2 (2003) 138–139.
[19] H.B. Yao, M.R. Gao, S.H. Yu, Small organic molecule templating synthesis of organic–inorganic hybrid materials: their nanostructures and properties, Nanoscale 2 (2010) 323–334.
[20] Y. Hakuta, S. Onai, H. Terayama, T. Adschiri, K. Arai, Production of ultra-fine ceria particles by hydrothermal synthesis under supercritical conditions, J. Materials Science Letters 17 (1998) 1211–1213.
[21] K. Byrappa, S. Ohara, T. Adschiri, Nanoparticles synthesis using supercritical fluid technology-towards biomedical applications, Advanced Drug Delivery Reviews 60 (2008) 299–327.
[22] J. Zhang, S. Ohara, M. Umetsu, T. Naka, Y. Hatakeyama, T. Adschiri, Colloidal ceria nanocrystals: a tailor-made crystal morphology in supercritical water, Advanced Materials 19 (2007) 203–206.
[23] E. Barraud, S. Bégin-Colin, G.L. Caër, F. Villieras, O. Barres, Thermal decomposition of $HfCl_4$ as a function of its hydration state, J. Solid State Chemistry 179 (2006) 1842–1851.
[24] V.P. Vasil'ev, A.I. Lytkin, N.V. Chernyavskaya, Thermodynamic characteristics of zirconium and hafnium hydroxides in aqueous solution, J. Thermal Analysis and Calorimetry 55 (1999) 1003–1009.
[25] J. Luo, L. Han, N.N. Kariuki, L. Wang, D. Mott, C.J. Zhong, T. He, Synthesis and characterization of monolayer-capped PtVFe nanoparticles with controllable sizes and composition, Chemistry of Materials 17 (2005) 5282–5290.
[26] S.S. Shankar, A. Rai, B. Ankamwar, A. Singh, A. Ahmad, M. Sastry, Biological synthesis of triangular gold nanoprisms, Nature Materials 3 (2004) 482–488.
[27] T. Adschiri, Y. Hakuta, K. Sue, K. Arai, Hydrothermal synthesis of metal oxide nanoparticles at supercritical conditions, J. Nanoparticle Research 3 (2001) 227–235.
[28] K. Sue, K. Kimura, M. Yamamoto, K. Arai, Rapid hydrothermal synthesis of ZnO nanorods without organics, Material Letters 58 (2004) 3350–3352.
[29] D. Rangappa, T. Naka, S. Ohara, T. Adschiri, Preparation of Ba-hexaferrite nanocrystals by an organic ligand-assisted supercritical water process, Crystal Growth and Design 10 (2010) 11–15.
[30] D. Chen, Y. Sugahara, Tungstate-based inorganic–organic hybrid nanobelts/nanotubes with lamellar mesostructures: synthesis, characterization, and formation mechanism, Chemistry of Materials 19 (2007) 1808–1815.
[31] J. Zhang, K. Sun, A. Kumbhar, J. Fang, Shape-control of ZnTe nanocrystal growth in organic solution, J. Physical Chemistry C 112 (2008) 5454–5458.
[32] D. Rangappa, T. Naka, A. Kondo, M. Ishii, T. Kobayashi, T. Adschiri, Transparent $CoAl_2O_4$ hybrid nano pigment by organic ligand-assisted supercritical water, J. American Chemical Society 129 (2007) 11061–11066.

ACS APPLIED MATERIALS & INTERFACES

Research Article

www.acsami.org

Supercritical Hydrothermal Synthesis and In situ Organic Modification of Indium Tin Oxide Nanoparticles Using Continuous-Flow Reaction System

Jinfeng Lu,[†] Kimitaka Minami,[†] Seiichi Takami,[‡] Masatoshi Shibata,[§] Yasunobu Kaneko,[§] and Tadafumi Adschiri*[,†,‡]

[†]Advanced Institute for Materials Research, WPI, and [‡]Institute of Multidisciplinary Research for Advanced Materials, Tohoku University

[§]Idemitsu Kosan Co., Ltd.

Supporting Information

ABSTRACT: ITO nanoparticles were synthesized hydrothermally and surface modified in supercritical water using a continuous flow reaction system. The organic modification of the nanoparticles converted the surface from hydrophilic to hydrophobic, making the modified nanoparticles easily dispersible in organic solvent. The addition of a surface modifier into the reaction system impacted the crystal growth and particle size as well as dispersion. The particle size was 18 nm. Highly crystalline cubic ITO with a narrow particle size distribution was obtained. The advantages of short reaction time and the use of a continuous reaction system make this method suitable for industrial scale synthesis.

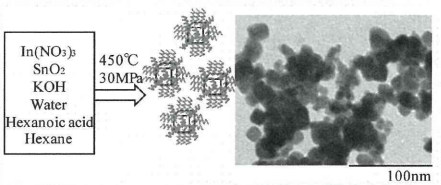

KEYWORDS: *ITO, supercritical condition, surface modification, nanoparticles, flow reaction system, environmentally benign technology*

INTRODUCTION

Tin-doped indium oxide (ITO) has been widely applied in photoelectronic products such as liquid-crystal displays (LCD), polymer electronics as organic photodiodes (OPD), thin film transistors (TFT), solar cells.[1−4] Its popularity arises from its properties of high electrical conductivity combined with high optical transparency in the visible spectral range, making it suitable for use as a transparent electrode which is fundamental in many optoelectronic devices.

ITO transparent electrodes traditionally have been deposited on flexible or heat-sensitive substrates using gas-phase deposition techniques.[5] However, with the rising price of indium metal and significant loss of ITO during conventional thin film deposition procedures, printing techniques such as inkjet printing that utilize ITO nanoparticles are expected to supplant the conventional method. Accordingly, interest in the production and use of ITO nanoparticles has steadily increased over the past few years. Using printing technology, ITO film can be fabricated more effectively and cheaply with less ITO loss.[6,7] When dispersing ITO nanoparticles into the ink, the inkjet printer can create an electric circuit directly onto the substrate. The critical issue in this type of printing technology is preparing nanosize particles, which can be homogeneously dispersed in a solvent.[8]

Typical transparent, electron conductive nanoink consists of ITO nanoparticles dispersed in solvent and mixed with a binder. Reducing the particle size to the order of nanometers improves the ITO film surface by diminishing haze and roughness and enhancing the transparency because of the suppression of Rayleigh scattering. The main difficulty lies in fabricating nanoparticles that will homogeneously disperse in solvent, as they tend to aggregate because of high surface energy. This property is adaptable through surface modification, which must be compatible with the rest of the fabrication process, including a low temperature curing. This has been problematic for particle films, as it has been reported that the sheet resistance of an ITO particle film after hardening under UV-irradiation at low temperature (<130 °C) was decreased to 1 kΩ /sq.[9] ITO nanoparticles are expected to help solve these problems, and may also improve upon the qualities of the conventional ITO coated films, which have only about 80% transmission in the visible light range.[10]

There have been several preparation methods of ITO nanoparticles reported, including low temperature coprecipitation, solvothermal synthesis, hydrothermal synthesis, and others.[11−16] However, there have been no methods developed that can maintain continuous production in an environmentally benign manner, and this is of crucial importance to establishing production at an industrial scale.

Supercritical continuous-flow reaction systems (SCFRS) offer a green route to producing metal oxide particles. A series of metal oxide nanoparticles has been synthesized in supercritical water.[17−19] Fang et al. synthesized nanocrystalline indium and tin oxide in supercritical water,[20] although the indium conversion rate was low (28.7%), they did not achieve a single phase ITO, nor did they attempt to utilize surface

Received: October 16, 2011
Accepted: December 1, 2011
Published: December 1, 2011

modification. In our group, we have established a novel process for the simultaneous synthesis and in situ modification of metal oxide nanoparticles under supercritical conditions.[21−23] We found that limiting crystal growth creates small, well-dispersed particles that resist aggregation, which can be accomplished by fabrication in supercritical water and modification with organic-ligand molecules. For this purpose, we employed this method of supercritical hydrothermal synthesis with SCFRS for the synthesis of well-dispersed ITO nanoparticles with a hydrophobic surface.

In this report, we describe the preparation and surface modification of highly crystalline ITO nanoparticles using organic molecules in supercritical water as the reaction medium. Additionally, we discuss dispersion and optoelectronic properties of these surface-modified ITO nanoparticles.

EXPERIMENTAL SECTION

$In(NO_3)_3$ was purchased from Shinko Chemical Co., Ltd. SnO_2 sol (8 wt %, pH =9.5−10.5, average of particle size: 2 nm) was from Taki Chemical Co., Ltd. KOH was from High Purity Chemicals Co., Ltd. Formic acid, hexanoic acid, and hexane were from Wako Chemicals, Ltd. The precursor solutions were prepared by dissolving $In(NO_3)_3$ and SnO_2 sol (molar ratio In:Sn = 9:1) in distilled water. To this mixture was slowly added KOH solution to obtain a white colored sol, the pH was adjusted to 7, and the precursor sol was diluted with distilled water to 0.1 M. 1.0 M formic acid in aqueous solution was prepared. Hexanoic acid used as modifier was dissolved in hexane to a concentration of 0.2 M.

The experiments were performed using a flow type stainless 316 steel reactor, as depicted in Figure.1. The system pressure was

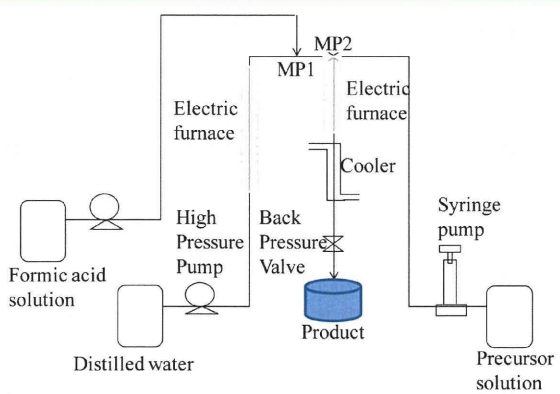

Figure 1. Schematic diagram of the flow reaction system.

maintained at 30 MPa using a backpressure regulator. Preheated high temperature water was fed into the reactor (36 mL/min) and mixed with 1.0 M formic acid fed from another line (4 mL/min) at mixing point 1 (MP1). Next, 0.1 M precursor sol or the mixture with modifier solution fed by the other line (4 mL/min) was added to this mixed solution at mixing point 2 (MP2). Subsequently, the solution was heated rapidly to the reaction temperature. The solution mixture was passed through a tube reactor and then quenched to room temperature by a cooling water jacket. The product solution was depressurized with a backpressure regulator and collected at the outlet. The reaction time (τ) was calculated based on the volume (V), flow rate (F), and density (ρ) of the solution in the tube reactor ($\tau = V/(F\rho)$). In this experiment, the reaction times for different temperature conditions were 22 s for 350 °C, 12 s for 400 °C, and 7 s for 450 °C.

The phases of the nanoparticles were characterized by X-ray diffractometry (XRD-Rigaku) using Cu Kα radiation. The particle size and morphology of the particles were examined using transmission electron microscopy (TEM(EDX)-Hitachi). The energy-dispersive X-ray (EDX) spectrum of samples was obtained using energy dispersive X-ray microanalysis (EDAX-AMETEK) combined with TEM. The electric resistance of the ITO samples was measured using a powder resistance measurement system (MCP-MCCAT). The conductivity was calculated from the measured resistance.

RESULTS AND DISCUSSION

As illustrated in Figure 1, the precursor sol was mixed with preheated water at MP2 to heat it rapidly to the reaction temperature (350, 400, and 450 °C). Figure 2A shows XRD

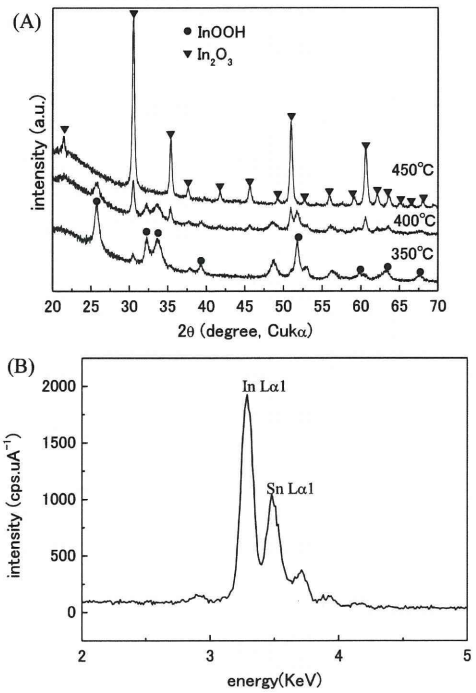

Figure 2. (A) XRD pattern of indium tin oxide (ITO) prepared at 350, 400, and 450 °C. (B) EDX spectrum of sample obtained at 450 °C.

patterns of samples obtained at these three temperatures. Temperatures below 400 °C produced mixed phases of cubic In_2O_3 and InOOH, but with increasing temperature, the peak of cubic In_2O_3 increased and that of InOOH became smaller, indicating a better yield of cubic In_2O_3. When the temperature was increased to 450 °C, a single phase was obtained. Compared with pure In_2O_3 (JCPDS Card No. 71−2195), the peaks were shifted to slightly lower values (Table S1 in the Supporting Information), indicating an increase in the size of the unit cell, indicating that Sn^{4+} might be doped into the cubic structure of In_2O_3.

In addition, EDX analysis of the nanoparticles was conducted combined with TEM image (Figure 4a). A typical EDX spectrum is shown in Figure 2B. Both In Lα1 (3.2 keV) and Sn Lα1 (3.4 keV) peaks were observed, indicating the presence of indium and tin elements in the products. The Sn/In ratio was determined to be 1:9, which matches the ratio in the precursor solution and provides further evidence of the formation of ITO. We also took the EDX analysis in other positions, which all showed the presence of tin.

XRD results suggest that InOOH nuclei form in the beginning of the reaction and upon dehydration generate

cubic In_2O_3. Temperature plays an important role in the formation of single phase ITO nanoparticles in the very short reaction time under supercritical conditions. Because of the remarkable decrease in water density as the temperature increases rapidly to 450 °C, the dehydroxylation from $In(OH)_3$ to InOOH and the final transformation to cubic In_2O_3 proceed rapidly. Conversely, at temperatures lower than 400 °C, the dehydration does not occur efficiently and thus the transformation from InOOH to In_2O_3 is incomplete.

In the next step in nanoparticle fabrication, to generate the reducing atmosphere needed for increasing the oxygen vacancy in ITO, formic acid solution was fed into MP1 where it combined with preheated supercritical water at 500 °C. Yu et al. has studied the thermal decomposition of formic acid at temperatures between 320 and 500 °C and pressures between 17.8 and 30.3 MPa,[24] and they reported that at 420 °C, the conversion of HCOOH reached 100% in a short reaction time to give the major products CO_2 and H_2. In supercritical water, the equilibrium of this reaction shifts toward the products CO_2 + H_2: H_2O + CO ⇆ HCOOH ⇆ CO_2 + H_2. These gases are miscible with supercritical water to form a homogeneous phase. Consequently, H_2 and CO_2 gases derived from the formic acid provide a good reducing atmosphere inside the tube reactor. Subsequently, the precursor sol was added into the reaction system at MP2 at a temperature of 450 °C. As shown in Figure

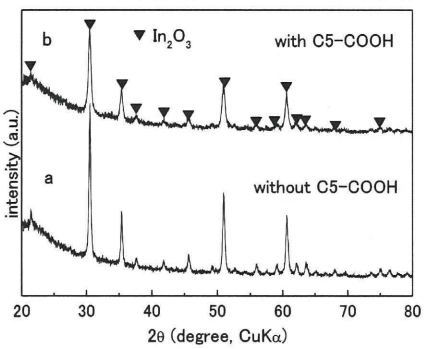

Figure 3. XRD patterns of ITO nanoparticles: (a) without modifier and (b) with modifier hexanoic acid (C5-COOH).

3, single-phase ITO was obtained under these conditions with no trace of additional phases. Furthermore, the color of the ITO nanoparticles changed from yellow to blue, which is a known indicator of a higher carrier concentration due to oxygen vacancies,[25] and is attributable to the reducing atmosphere generated by the addition of formic acid. TEM was used to assess the size of the blue ITO nanoparticles (Figure 4), which were found to be ~30 nm. However, TEM also revealed that the ITO nanoparticles were heavily aggregated, and so we proceeded to carry out in situ surface modification in the SCFRS.

Hexanoic acid solution was added to the precursor sol in a 1:2 ratio and stirred rigorously. The other conditions were kept the same, i.e., the reaction temperature was 450 °C and pressure was 30 MPa, and formic acid was again added to create a reducing atmosphere. The effect of introducing hexanoic acid into the system was that the organic ligand capped the nanoparticle surface and limited the growth of the particles. The XRD pattern of modified nanoparticles reveals that all of the peaks are lower in intensity and broadened as compared

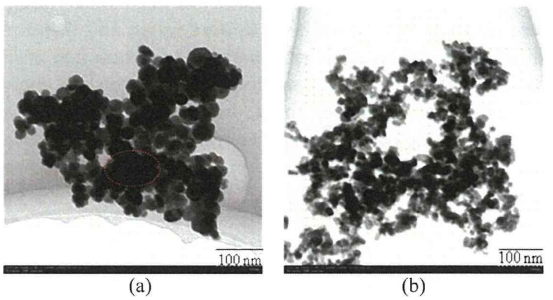

Figure 4. TEM images of samples (a) without modifier and (b) with modifier hexanoic acid. Red circle shows the region of EDX analysis.

with the pattern of nanoparticles fabricated without organic surface modification (Figure 3). The crystallite sizes of these two samples were calculated from the main peak (hkl = 222) of XRD data using Scherrer's equation; the unmodified nanoparticles were found to be 32 nm and the nanoparticles modified with hexanoic acid were 18 nm, demonstrating that the size of the nanoparticles was reduced by the organic ligand capping. This smaller size of the modified particles was confirmed using TEM. From the image of the modified nanoparticles (Figure 4), the size was found to be consistent with the XRD (hkl = 222 peak is significantly high) results, revealing cubic ITO particles with an average diameter of 18 ± 0.8 nm.

The dispersibility of ITO was investigated by putting the particles in a binary phase-separated solvent of hexane and water. As shown in Figure 5, the surface modified particles

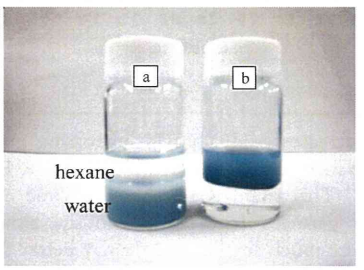

Figure 5. Dispersibility of ITO nanoparticles (a) in the absence of organic modifier and (b) in the presence of organic modifier hexanoic acid.

dispersed in organic phase, whereas the particles without surface modification dispersed in the aqueous phase of the binary solvent system. These results indicate that the organic ligand, hexanoic acid, had bound to the surface of modified ITO nanoparticles and converted them from hydrophilic to hydrophobic, although hexanoic acid may not be the best modifier.[15] We have succeeded in making a thin film by the spin-coating method for well-dispersed nanoparticles, although we have not measured the electroconductivity of the film.

For this system, it is worthwhile to understand the phase behavior and the solvent effect on the nucleation rate in the presence of organic capping agent. It is known that in the supercritical region, water becomes completely miscible with many hydrocarbons while also becoming a poor solvent for many inorganics.[26] From the pressure–temperature phase diagram for the water and hexane mixture, it is known that the mixture will become one phase above 360 °C at 30 MPa.[27]